Significance of extracellular polymeric substances, reactive oxygen species, and expression of extracellular electron transfer genes on methanogenic activity in biocathode

Basem S. Zakaria, Bipro Ranjan Dhar*

Civil and Environmental Engineering, University of Alberta, 9211-116 Street NW, Edmonton, AB, Canada T6G 1H9

*Corresponding author: bipro@ualberta.ca (B.R. Dhar)

Abstract

This study presents a multifaceted approach combining characterization of microbial communities, extracellular polymeric substances (EPS), reactive oxygen species (ROS), and expression of genes associated with extracellular electron transfer (EET) to shed light on their significance on electro-methanogenic activity in different biocathode materials. Carbon fiber and stainless-steel mesh biocathode were tested in microbial electrolysis cell assisted anaerobic digestion (MEC-AD) systems fed with synthetic glucose medium. Despite the higher specific surface area provided by carbon fiber biocathode, methanogenesis performance was much inferior (100.3 mL CH_4) than that obtained from a stainless steel biocathode (179.5 mL CH_4) operated under the same operating conditions. Interestingly, biofilms did not entirely cover the surfaces of carbon fibers, while stainless steel biocathode showed evenly denser biofilms with higher biovolume (30.2±4.2 vs. 13.5±2.8 $\mu m^3/\mu m^2$). Analyses of microbial communities indicated that the key mechanism for electro-methanogenesis in both reactors was hydrogenotrophic methanogenesis by *Methanobacterium* species. Along with the effective catalysis of hydrogen evolution reaction (HER), a higher abundance of known hydrogenotrophic *Methanobacterium* sp. and homoacetogenic *Acetobacterium* appeared to play a major role in superior methanogenesis on stainless steel biocathode. The most considerable secretion of EPS accompanied by the lowest ROS level in stainless steel biocathode indicated that higher EPS possibly protected cells from harsh metabolic conditions (e.g., unfavorable local pH) induced by faster HER. Moreover, the redox activity of EPS derived from biocathode, as well as expressions of EET genes, suggested that electro-methanogenesis via direct electron transfer might have occurred to some extent in both biocathodes. Overall, the results of this study have important significance in the development of effective biocathode for MEC-AD systems.

Keywords: Electro-methanogenesis; Biomethane; Biocathode; Extracellular polymeric substance (EPS); MEC-AD

1. Introduction

The concept of electro-methanogenesis by combining the microbial electrolysis cell (MEC) and anaerobic digestion (AD) has become a promising method for process intensification and improving the stability of digesters [1–5]. The integrated process is called microbial electrolysis cell assisted anaerobic digester (MEC-AD). In MEC-AD systems, methane can be produced via multiple pathways. For instance, methane can be produced in biocathode through (1) direct electron transfer from the electrode to electrotrophic methanogens coupled with CO_2 reduction to methane, and (2) hydrogenotrophic methanogenesis of H_2 produced via hydrogen evolution reaction (HER) [4–7]. Moreover, methane can also be produced via direct interspecies electron transfer (DIET) between electroactive bacteria and electrotrophic methanogens in both cathode and anode electrodes [7–9]. Nonetheless, a considerable portion of methane would still be generated via conventional acetoclastic and hydrogenotrophic methanogenesis pathways.

The activity of anodic electroactive bacteria (EAB) was identified as one of the key factors for boosting the methanogenesis process in MEC-AD systems. Remarkably, EAB can outcompete acetoclastic methanogens due to faster growth kinetics [10]. Thus, EAB can divert electrons from acetate to anode via extracellular electron transport (EET). The transferred electrons can be utilized for hydrogen production via a cathodic HER. Thus, fast-growing hydrogenotrophic archaea can be augmented on the biocathode. Several studies revealed enrichment of known hydrogenotrophic methanogens, such as *Methanobacterium* and *Methanobrevibacter* in the cathode, which corroborated faster methanogenesis rates in MEC-AD systems over conventional digesters [8–11].

While many studies emphasized the importance of a kinetically efficient electrode-attached microbiome in MEC-AD systems, studies documented the significance of extracellular polymeric substance (EPS) in biocathode are limited. Biofilm EPS can have many functions, including attachment of cells to solid surfaces, maturation of biofilm structures, and protection of cells from harsh environmental conditions [12–14]. A few recent studies validated the significance of EPS in EET within anode biofilms in various bio-electrochemical systems [14–17]. In general, EPSs are composed of proteins, DNA, humic acids, polysaccharides, etc., that are secreted by microbes in pure and mixed cultures, which facilitate biofilm growth and protection under unfavorable metabolic environment [13,14]. Notably, various EPS components, including humic acids, extracellular DNA (eDNA), and heme-binding proteins, showed redox properties, which could serve as an immobilized mediator (i.e., electron carrier) in electrochemically active biofilms [14,16,17]. Interestingly, EPS extracted from anaerobic digester has now been shown to have redox properties and identified as an essential route for DIET between syntrophic bacteria and methanogens [18,19]. As direct electron transport from the cathode-to-methanogen and bacteria-to-methanogens can promote methanogenesis in biocathode, it can be assumed that EPS in biocathode can potentially be linked with MEC-AD performance. However, to the best of the authors' knowledge, there is no published literature reporting the characteristics and significance of biocathode EPS and expressions of EET genes in MEC-AD systems.

The optimization of applied voltage/potential and inoculation method has been broadly investigated to enrich a syntrophically balanced microbial communities towards developing MEC-AD systems [2,20]. Previous studies also substantiated the importance of persuasive system design for effective electro-methanogenesis [21–23]. Particularly, the selection of cathode electrode with low overpotential, large effective surface area, and good conductive properties was found to play a

deterministic role in MEC-AD performance [3,24–26]. However, carbon based-cathode materials, such as carbon fiber, carbon cloth, and carbon brush, have been employed in most of the previous studies due to their high surface area and biocompatibility properties [3,24,26]. However, carbon-based electrodes provide slow catalysis for cathodic HER, which seems to be critical for enriching hydrogenotrophic methanogens [1,24,27]. Some previous studies successfully employed metal catalyst on carbon electrodes, such as nickel- and platinum-coated carbon materials, to provide superior HER [1,24,27], while these catalysts are still quite expensive. In contrast, non-precious metal electrodes, such as stainless steel, have shown an excellent low-cost alternative to promote HER [11,25,28–30]. However, to date, limited information is available on how carbonaceous and metal-based electrodes shape biocathode structures in terms of EPS, expression of EET genes, and microbial communities.

Considering the research gaps mentioned above, the main goal of this study was to provide fundamental insights into the EPS as well as microbial communities that drive methanogenesis in biocathode developed on carbon and metal electrode surface. The novelty of this study is two folds: (1) This study presents, for the first time, the complete characterization of methanogenic biocathode EPS and expression of EET genes in MEC-AD systems; (2) This study presents a comparison between carbonaceous and metal electrodes based on a multifaceted approach combining molecular biology, microscopic, and electrochemical tools to link the structures and compositions of biocathode EPS and microbial communities with their methanogenesis performance.

2. Materials and methods

2.1. MEC Start-up and operation

Two single chamber MEC-AD systems (working volume of 360 mL), constructed with plexiglass, were used in this experiment. Carbon fibers (2293-A, 24A Carbon Fiber, Fibre Glast Development Corp., Ohio, USA) fixed onto a stainless steel frame (which was not exposed to the liquid medium) was used as an anode electrode in both reactors. A similar carbon fiber module was used as a cathode electrode in one reactor (referred to as 'CF-CF'), and a stainless steel mesh (304 stainless steel, McMASTER-CARR, USA) was used as a cathode electrode in the other reactor (referred to as 'CF-SS'). The specific surface area provided by the stainless-steel electrode was 4.2 m^2/m^3. Considering every single filament in the carbon fiber bundle, the specific surface area of the carbon fibers module was estimated at 3609 m^2/m^3. Moreover, considering all filaments in a bundle act together as a single fiber, the surface area was estimated at 41 m^2/m^3. The detailed calculation of the specific surface areas for carbon fibers and stainless-steel electrodes are provided in the Supplementary Information. The Ag/AgCl reference electrode (MF-2052, Bioanalytical System Inc., USA) was positioned close (<1 cm) to the anode electrode.

Both reactors were inoculated with mesophilic anaerobic digester sludge and effluent from a dual-chamber mother MEC that has been operated with sodium acetate as a sole electron donor for over 12 months. Initially, sodium acetate (1600±55 mg COD/L) supplemented phosphate buffer (50 mM) and trace minerals were used as a substrate. The detailed information regarding the trace minerals can be found elsewhere [2]. The reactors were operated with acetate in fed-batch mode until peak current densities for both reactors reached ~77 A/m^3. Then, the substrate was switched to glucose (2150±31 mg COD/L), while buffer and trace minerals composition remained the same. With glucose medium, reactors were operated for about six months under batch mode in repetitive cycles. The biogas produced from the reactors were collected into gasbags. A decrease in daily methane production to <3 mL was considered as an indicator for replacing the substrate medium.

During experiments, a multi-channel potentiostat (Squidstat Prime, Admiral Instruments, Arizona, USA) was used to fix the anode potential at -0.4 vs. Ag/AgCl. The reactors were operated at room temperature 21±1°C with continuous mixing of the liquid medium with magnetic stirrers at 130±5 rpm.

2.2. Characterization of EPS

For the quantitative analysis of EPS, biomass samples were washed three times with 0.1 M PBS (pH 7.4), and then the supernatant was removed after centrifugation at 3000 × g for 15 min at 21ºC. EPS extraction was performed using two methods; cation-exchange resin (CER) and heating method, to examine the effect of different EPS extraction methods. The details of EPS extraction and analytical methods for various EPS components (proteins, carbohydrates, eDNA, heme-binding proteins, and uronic acid) were provided in the Supplementary Information. Both EPS extraction methods (CER and heating method) provided similar results (see Supplementary Information). Hence, we reported the results from the CER method.

Confocal laser scanning microscopy (CLSM) was used to visualize and examine the EPS structure on the electrodes. Portions of carbon fibers and stainless-steel mesh were cut with an aseptic scissor from different locations and washed with 0.1 M PBS buffer (pH 7.4) to remove any debris. The electrodes were fluorescently stained with TOTO™-1 (Thermo Fisher, USA) and Concanavalin A (ConA) Alexa Fluor™ 633 Conjugate (Thermo Fisher, USA) for one hour in the dark for eDNA and EPS visualization, respectively. Then, the samples were washed again with PBS buffer to remove any non-specific binding stains. The stained electrodes were placed on MatTek dishes with a 1.5 coverslip (MatTek co., USA) to ensure that the biofilm was not compressed. The visualization of the electrodes was performed using a Leica inverted DMI 6000 B microscope (Leica Microsystems, USA). CLSM was equipped with an argon laser and helium-neon lasers. The

images were acquired using x63/1.3 water immersion lens using LAS AF software (Leica Microsystems, USA) at a resolution of 1024 x 1024 with 120 nm pixel size. Images z-stack were acquired with several steps 29 with z-step size 0.29 µm with smart grain 687. The quantitative analysis of EPS structure was carried out using biofilm image processing COMSTAT software. The EPS intensities were reported as intensity/um^3 of the electrode.

The electrochemical characteristics of extracted EPS from cathodic biofilms was further analyzed with low-scan cyclic voltammetry under three-electrode (working, counter, and reference) configuration. After extraction, 2 mL of extracted EPS was transferred to an electrochemical cell having screen printed electrodes (A-AD-GG-103-N, Zimmer and Peacock Ltd., Royston, UK). The working electrode voltage was ramped between −0.8 and 0.8 V vs. Ag/AgCl at a scan rate of 1 mV/s using the potentiostat (Squidstat Prime, Admiral Instruments, USA), and current was recorded every 1 seconds.

2.3. Microscopic imaging of biofilms

Microscopic visualization of anode and cathode biofilms was performed using a scanning electron microscope (Carl Zeiss, Cambridge, UK). Several images from different locations of electrodes were captured. The detailed protocol of sample preparation and imaging could be found elsewhere [13].

2.4. Analysis of reactive oxygen species (ROS)

The levels of reactive oxygen species (ROS) in biofilms were visualized using CLSM. We collected different parts of electrodes, then washed three times using 0.1 M PBS to remove any debris. Samples were stained with 2',7'-Dichlorofluorescein diacetate (10 µM) (Thermo Fisher, USA) for one hour. The visualization was then performed using CLSM (as mentioned earlier) with

excitation and emission wavelength; 495 nm and 520 nm, respectively. The quantitative analysis of ROS levels was carried out using image processing COMSTAT software.

2.5. Microbial communities and gene expression analyses

For the characterization of microbial communities, genomic DNA was extracted using PowerSoil® DNA Isolation Kit (MoBio Laboratories, Carlsbad, USA) according to the manufacturer's instructions from the anode and cathode biofilm. The purity and concentration of DNA was measured with Nanodrop spectrophotometer (Model 2000C, Thermo Scientific, USA). The extracted DNA was stored immediately at -70 ˚C prior to the sequencing. Illumina Miseq Sequencing was performed by the Research and Testing Laboratory (Lubbock, TX, USA) targeting 16S rRNA gene using bacterial primers 341F: 5' CCTACGGGNGGCWGCAG 3' and 805R: 5' GACTACHVGGGTATCTAATCC 3' [31,32], archaeal primers 517F: 5' GCYTAAAGSRNCCGTAGC 3' and 909R: 5' TTTCAGYCTTGCGRCCGTAC 3' and specific *mcr*A archaeal primers *mcr*Af: 5' GGTGGTGTMGGATTCACACARTAYGCWACAGC 3' and *mcr*Ar: 5' TTCATTGCRTAGTTWGGRTAGTT 3' [33].

For evaluation of microbial diversity, the nucleotide sequence reads were sorted out using a data analysis pipeline. Short sequences, noisy reads and chimeric sequences were removed through a denoising step and chimera detection, respectively. Then, each sample was run through the analysis pipeline to establish the taxonomic information for each constituent read. Microbial taxonomy was assigned using the Quantitative Insights Into Microbial Ecology (QIIME) pipeline (http://qiime.org [34])[34]. Principal component analysis (PCA) of bacterial and archaeal communities on cathode electrodes of CF-CF and CF-SS was conducted using weighted Unifrac metrics to show the relation between genera and PCs.

The expression of EET-associated genes (i.e., *pil*A, *omc*B, *omc*C, *omc*E, *omc*Z, and *omc*S) were quantified. The primers and design method used in this study are listed in the Supplementary Information. Total RNA was extracted using RNeasy PowerSoil Total RNA Kit (Qiagen, CA), then the purity and concentration were examined using Nanodrop (2000C, Thermo Scientific, USA). Subsequently, cDNA synthesis was performed using QuantiTect Reverse Transcription Kit (Qiagen, CA). Then, RT-PCR mixtures were prepared in 25 uL reactions using QuantiFast SYBR® Green PCR Kit (Qiagen, CA) as the following: 1 µL of the template, 12.5 µL 2x master mix, 2.5 µL forward and reverse specific primer, and 6.5 µL nuclease-free water. CFX 96 real-time PCR system with a C1000 Thermal Cycler (Bio-Rad, USA) was used with the following cycling conditions according to the QuantiFast SYBR® Green PCR Kit's protocol; PCR initial heat activation cycle at 95 ˚C for 5 min, 35 cycles at 95 ˚C for 10 sec and 60 ˚C for 30 sec, and finally, one cycle at 40 ˚C for 30 seconds. Triplicate reactions were run for all samples.

2.6. Analytical methods

Current and applied voltage/potential were recorded every 4.8 min using a computer connected with the multi-channel potentiostat (Squidstat Prime, Admiral Instruments, USA). The liquid samples from reactors were filtered with syringe filters (0.45 µm) for chemical oxygen demand (COD) measurements. The COD concentrations were measured with HACH Chemical method using UV-spectrophotometer (Model DR 3900, HACH, Germany). A bench-top pH meter (Accumet AR15, Fisher Scientific, Pittsburgh, PA, USA) used for pH measurement. The concentrations of various volatile fatty acids, VFAs (acetate, propionate, and butyrate) were measured with an ion chromatography (DionexTM ICS-2100, Thermo Scientific, USA); the detailed operating protocol could be found elsewhere [35]. The biogas produced from reactors was collected with 500 mL gas bags. The composition of biogas (i.e., methane content) was analyzed

by a gas chromatograph (7890B, Agilent Technologies, Santa Clara, USA) equipped with a thermal conductivity detector (TCD) and two columns (Molsieve 5A and Hayesep). To reveal the statistical difference between the results collected from two reactors, the student's paired t-test (JMP® Software, SAS, US) was used.

3. Results and discussion

3.1. MEC-AD performance

The performances of MEC-AD systems were compared in terms of current density and methane productivity. Fig. 1a shows the volumetric current densities from two configurations. The maximum volumetric current density from the CF-SS reactor reached 34.1±0.3 A/m^3, which was significantly higher (p=0.01) than that of CF-CF (27.6±0.2 A/m^3). Fig. 1b shows the methane production profiles during batch operation. Although the methane generation patterns were comparable in both reactors, CF-SS showed higher (p=0.03) daily methane production than CF-CF throughout the batch cycle (Fig. 1b). Also, the total cumulative methane production was substantially higher in CF-SS (179.5±6.7 vs. 100.3±7.9 mL CH_4; p=0.01). Both reactors were operated under identical operating conditions (e.g., mixing speed, inoculation, etc.). Furthermore, considering that the carbon fibers module was used as the anode electrode in both reactors, the differences in system performance could be closely tied to the difference in the cathode electrode. As discussed later, stainless steel mesh cathode in the CF-SS reactor facilitated denser biofilms formation with more methanogenic biomass with higher EPS levels.

It is interesting to note that electrodes providing high specific surface areas have been reported to be efficient for enhancing the electrochemical performance of various bio-electrochemical systems [3,22,24–26]. Therefore, carbon-based electrodes, such as carbon brush, activated carbon, have been widely used for various biocathode applications, including electro-methanogenesis [3,24,26]. Notably,

the rough surface of carbon fiber was found to be efficient for developing electrochemically active biofilms [36]. Although we cannot rule out that different textures (diameter of carbon fiber and steel wire) could also lead to distinct colonization of biomass [37,38], the specific surface area provided by electrodes is often considered a critical factor in designs of bio-electrochemical systems. It appeared that stainless steel mesh cathode having a relatively lower specific surface area than carbon fibers (4.23 vs. 3609 m^2/m^3) resulted in superior methanogenic activity from CF-SS. It has been previously suggested that the agglomeration of fibers in the liquid phase could reduce the available specific surface area for biofilms formation [39]. Nonetheless, considering all carbon fiber filaments in a bundle as a single fiber, the specific surface area provided by the carbon fiber biocathode was still higher than the stainless-steel cathode (4.23 vs. 41 m^2/m^3).

Carbon-based electrodes are considered inferior catalysts for HER compared to metal and carbon-metal composite electrodes [11,25,28–30]. Most of the previous single-chamber MEC-AD studies substantiated the role of hydrogenotrophic methanogenesis on the biocathode. Also, it is reasonable that acetoclastic methanogens would likely be washed out at low hydraulic residence time (<7 days) used in this study [7,40]. Thus, the inferior methane recovery from the CF-CF reactor as compared to the CF-SS reactor was likely due to the inferior catalytic activity of carbon fibers for HER and subsequent indirect electro-methanogenesis (i.e., hydrogenotrophic methanogenesis of hydrogen produced via HER).

3.2. Organics removal and VFAs profiles

As shown in Fig. 2a, the effluent COD concentration from CF-SS (215±2.8 mg/L) was considerably lower ($p=0.001$) than that of CF-CF (382±3.0 mg/L). Correspondingly, the COD removal efficiencies were 89.9±0.5% and 83±1.7% in CF-SS and CF-CF, respectively. Thus, the COD removal efficiencies also showed similar trends with volumetric current density and methane

production. Fig. 2b and 2c show the changes in VFAs concentrations during batch operation. For both reactors, the acetate concentrations were relatively higher than propionate and butyrate concentrations during the operational period. The CF-SS reactor showed the highest acetate concentration of 439±2 mg COD/L, while propionate (94±0.1 mg COD/L) and butyrate (61±0.3 mg COD/L) concentrations were relatively lower. In contrast, CF-CF exhibited the highest acetate concentration of 320±0.4 mg COD/L, which was lower than that of the highest acetate concentration observed in CF-SS. Propionate concentrations were relatively higher in CF-CF, with the highest concentration of 118±0.4 mg COD/L. The highest butyrate concentration (64.8±1.3 mg COD/L) in CF-CF was comparable to CF-SS (61±0.3 mg COD/L). CF-SS also showed a lower accumulation of VFAs in the final effluent, as compared to CF-CF (52.6±0.5 vs. 133.5±1.0 mg COD/L; p=0.005).

Throughout the batch operation, propionate concentrations in CF-SS remained relatively lower than those observed in CF-SS, indicating faster conversion of propionate in the CF-SS. The fermentation of propionate to acetate is a vital process towards anodic respiration by EAB as well as acetoclastic methanogenesis. However, propionate fermentation to acetate is energetically unfavorable in terms of Gibbs free energy [41]. Thus, maintaining lower hydrogen partial pressure would be critical for propionate fermentation to acetate. Even though stainless-steel cathode would be expected to provide superior HER compared to the carbon fibers [11,29], no hydrogen was detected in biogas collected from both reactors. This might be due to the rapid consumption of hydrogen by hydrogenotrophic methanogens, as suggested in previous studies [11,42]. Moreover, enhanced homoacetogenic activity ($H_2 + CO_2 \rightarrow$ acetate) could play a role in maintaining lower hydrogen partial pressure in biocathode [11,42]. As discussed later, microbial community analysis also coincided with these notions. Thus, the comparison of VFA profiles suggests that microbial

communities in the CF-SS reactor more rapidly utilized hydrogen produced via fermentation and cathodic HER.

3.3. EPS structures and characteristics

Fig. 3 shows that carbohydrates, proteins, and heme-binding proteins were the major components of EPS extracted from biofilms in both reactors. The EPS composition of the anode biofilms in both reactors was quite similar and was not affected by the different cathode materials used in the two configurations. Protein was found as the major EPS component in anode biofilms in this study, which is consistent with recent reports on EPS composition in pure culture *Geobacter* biofilms [17,43]. *Geobacter* species were also abundant in anode biofilms of both reactors in this study (discussed later). The concentrations of major EPS components (carbohydrates, proteins, and hemes) in the cathode biofilms in CF-SS were higher than those of CF-CF. Notably, carbohydrates (52.2±0.2 mg/cm^2) and proteins (212.8±3.4 mg/cm^2) concentrations were markedly higher in CF-SS, as compared to cathode biofilms in CF-CF (carbohydrates: 25.8±0.5 mg/cm^2; proteins: 170±1.3 mg/cm^2). The heme-binding proteins (CF-CF: 16.5±0.4 mg/L; CF-SS: 34.2±2.3 mg/L), uronic acid (CF-CF: 6.2±1.0 mg/L; CF-SS: 15±0.2 mg/L) and eDNA (CF-CF: 0.39±0.01 mg/L; CF-SS: 1.5±0.05 mg/L) also showed same patterns. Overall, cathodic biofilms developed on the stainless-steel electrode exhibited markedly higher EPS levels ($p=0.03$).

To further verify EPS measurement results, electrode surfaces were visualized with CLSM (see Fig. 4) to quantify EPS intensity and biovolume of biofilms. The CLSM images showed that EPS was more uniformly distributed on the stainless-steel cathode surface in CF-SS than the carbon fiber electrodes in both reactors. As shown in Fig. 5a, the biovolume of cathode biofilms in CF-SS was estimated at 30.2±4.2 μm^3/μm^2, which was two times higher than the biovolume estimated for cathode biofilms in CF-CF (13.5±2.8 μm^3/μm^2). However, biovolumes estimated for anode

biofilms in both reactors were comparable (p=0.007). The intensities of EPS and eDNA were also quantified (Fig. 5b). Like estimated biovolume, EPS and eDNA intensities in cathode biofilms on stainless steel were higher than those estimated for cathode biofilms in the CF-CF reactor (p=0.008). At the same time, EPS and eDNA intensities were comparable for anode biofilms in both reactors (p=0.20). Thus, CLSM imaging and COMSTAT analysis further confirmed that the stainless-steel cathode resulted in the highest EPS production.

Studies associated with the role of EPS in the performance of bio-electrochemical systems received less attention and primarily focused on anode biofilms and their interrelationships with electrocatalytic activity (i.e., current density). A few studies revealed that EPS extracted from biofilms of electroactive *Geobacter sulfurreducens*, *Shewanella oneidensis* and *Pseudomonas putida* were electrochemically active [14,17,43]. Notably, EPS-associated proteins with redox-active features are a significant contributor to the EET from EAB to the anode [14,17,43]. Moreover, higher levels of redox-active proteins in anode biofilms were correlated with higher EET efficiency. Interestingly, despite differences in volumetric current densities, both EPS composition and concentrations were quite similar in anode biofilms in both reactors. Instead, the difference in EPS levels in cathode biofilms was likely linked to volumetric current densities and methane production. Interestingly, a recent study demonstrated that the addition of iron-based conductive materials in conventional anaerobic bioreactors could enhance EPS contents in methanogenic biomass [18], which was positively correlated with methane generation rates. Conductive materials promote the syntrophic DIET from bacteria to archaea and thereby enhance methanogenesis [44]. Therefore, to get more insights, the CV of extracted EPS was performed to qualitatively identify the redox activity of cathodic EPS. As shown in Fig. 6, voltammograms of cathodic EPS extracted from both reactors showed distinct redox peaks, suggesting the redox capability of EPS in both

biocathodes. However, redox peaks were observed at different potential, indicating that redox properties would be different for EPS extracted from different cathode electrodes. Moreover, the peak current from the EPS extracted from stainless steel biocathode was considerably higher than the EPS extracted from carbon fiber biocathode. This difference could be associated with higher concentrations of redox-active EPS in stainless steel biocathode; however, future investigation is warranted to reach a more thorough understanding of their redox characteristics.

A recent study reported that the current generated from anode biofilms was positively associated with EPS protein content and negatively correlated to carbohydrates in EPS [45]. In this study, both carbohydrates and proteins were considerably higher in EPS extracted from stainless steel biocathode than that of carbon fiber biocathode. The secretion of carbohydrates could be associated with harsh environmental conditions [13,19]. More secretion of carbohydrates can provide a protective layer and maintain the redox activity of proteins involved in EET [16,19]. It is possible that enhanced HER with a stainless steel cathode could create highly alkaline conditions near the cathode surface [7,46,47], which might induce more EPS secretion. Based on a recent report, hydrogenotrophic methanogenesis could be the dominant pathway under alkaline pH [48]. As discussed later, biofilms grown on stainless steel cathode showed a higher abundance of hydrogenotrophic methanogens in this study. While further investigation is needed to understand the function of various EPS on electro-methanogenesis, the results suggested that cathodic electrode material could considerably influence biofilm growth/composition along with EPS secretion, and ultimately the methane productivity and kinetics from MEC-AD systems.

3.4. ROS levels in biofilms

The quantitative measurement of ROS levels in biofilms was performed with CLSM imaging (see Supplementary Information), which showed a difference in the ROS level between biofilms grown

on stainless steel and carbon fibers (Fig. 7). The lowest ROS level was observed for cathode biofilms on stainless steel surface, while very similar ROS levels were found in anode/cathode biofilms developed on carbon fibers. Recent studies reported ROS accumulation in the anaerobic digestion process [15,49], while ROS is usually thought to be produced during aerobic metabolism. It has been suggested that unfavorable metabolic conditions (e.g., inhibition by toxicants, pH changes) could lead to ROS accumulation in digesters [15,49]. For instance, superior HER on stainless steel could induce local alkaline pH in biocathode. ROS accumulation may suppress metabolic activities, leading to the deterioration of digester performance. The lowest ROS level in biocathode developed on stainless steel suggests that higher EPS levels provided some degree of protection to the cathodic microbiome from potential environmental stress (e.g., pH changes). However, potential mechanisms relating to EPS and ROS levels should be further explored.

3.5. Microbial quantity and diversity

Fig. 8 shows the quantitative assessment of microbial communities performed with qPCR. The total microbial cell counts (16S) in anode biofilms in CF-SS (9×10^8 cells/cm^2) were slightly higher than that of CF-CF (8×10^8 cells/cm^2) (Fig. 8a). An almost similar pattern was observed for cathode biofilms; however, the difference was more prominent (CF-SS: 1×10^{11} cells/cm^2; CF-CF: 6×10^8 cells/cm^2). The archaeal cell numbers also showed similar patterns, with the highest archaeal cell numbers for the stainless steel biocathode. In addition, *mcr*A gene copies were quantified to elucidate the archaeal cell numbers; the *mcr*A gene is considered as a biomarker for methanogens [50]. Sequencing of the *mcr*A gene was used in a few studies to understand the taxonomy of methanogens [33,50,51]. A few recent reports also confirmed the positive link between *mcr*A gene copies and methanogenesis rates in MEC-AD reactors [33,50,51]. The highest *mcr*A gene copy numbers were observed for the cathodic biofilm in CF-SS (4×10^6 cells/cm^2), as compared to the

CF-CF reactor (4×10^4 cells/cm^2) (Fig. 8b). The *mcr*A gene copy numbers in anodic biofilms for both systems were comparable (CF-CF: 1.3×10^4 cells/cm^2; CF-SS: 1.8×10^4 cells/cm^2). Thus, the enhanced methane recovery from the CF-SS reactor can be explained by the higher abundance of *mcr*A gene copies within the stainless steel biocathode.

Fig. 10 shows microscopic images of biofilms, which show the differences in structures of biofilms developed on different electrodes. The anode/cathode biofilms grown on carbon fibers exhibited substantial heterogeneity (Fig. 10). Also, it can be clearly noticed that biofilms did not fully cover the surfaces of carbon fibers. SEM imaging revealed that biofilms grown on stainless steel cathode in CF-SS was evenly denser than anode/cathode biofilms grown on carbon fiber electrodes (Fig. 10), suggesting the large secretion of EPS accelerated the surface attachment of cells on the stainless steel electrode. Thus, SEM imaging also corroborates the qPCR and CLMS results.

The alpha diversity of anode and cathode biofilms was also estimated. The numbers of Chao 1, phylogenetic distance, OTUs, Pielou's evenness, and Shannon index were provided in the Supplementary Information. The results clearly showed that the richness and diversity indices were relatively higher in CF-SS. Notably, cathode biofilms in CF-SS showed more diversity with the Shannon index of 5.10, as compared to CF-CF (3.95). These results indicated that the stainless-steel electrode persuaded the richness and diversity of the microbial communities.

3.6. Microbial community composition, and gene expression

3.6.1. 16S rRNA sequencing

Microbial communities in two reactors were analyzed with specific bacterial, archaeal, and *mcr*A primers. At the phylum level, Proteobacteria was the most abundant in anode biofilms in both reactors; however, its relative abundance was much higher in CF-SS than CF-CF (85% vs. 47%)

(see Supporting Information). The relative abundances of Bacteroidetes and Firmicutes in CF-CF were 26% and 14%, which were considerably higher than that of CF-SS (6% and 4%, respectively). Also, Synergistetes (6%) and Lentisophaerae (4%) were present at slightly higher abundances in CF-CF, while in CF-SS, they were 1% and 3%, respectively. Similar to anode biofilms, Proteobacteria was the most abundant in cathode biofilms in both reactors. However, its relative abundance was comparable in both configurations; recorded 64% and 68% of CF-CF and CF-SS, respectively. However, the abundance of Bacteroidetes was higher in CF-CF (17%) than CF-SS (6%). On the contrary, Firmicutes (20%) was the second most abundant member in CF-SS, while their abundance in CF-SS was considerably lower (9%).

At the genus level, *Geobacter,* belong to Proteobacteria, was the most abundant in anode biofilms in both systems with 22% and 59% in CF-CF and CF-SS, respectively (Fig. 9a). *Geobacter* is a highly efficient electroactive microorganism that has the capability to utilize simple organic acids like acetate and were widely dominant on the anode biofilm in most of the previous studies [35,45]. In CF-CF, *Bacteroides* was the second most dominant genus (12%), followed by *Enterobacteriaceae* (10%) and *Dysgonomonas* (5%). In contrast, the second abundant genus in CF-SS was *Enterobacteriaceae* (23%), followed by *Dysgonomonas* (3%) and *Victivallis* (3%).

The cathode biofilms in both reactors are dominated by the members of *Enterobacteriaceae* genus (CF-CF: 42%; CF-SS: 60%). On the cathode electrodes, *Bacteroides* (12%), *Pleomorphomonas* (9%), and *Desulfovibrio* (4%) were the other dominant genera in CF-CF. In contrast, *Acetobacterium* was the second abundant genus (16%), followed by *Bacteroides* (5%), *Dysgonomonas* (3%), and *Desulfovibrio* (2%) in CF-SS. *Acetobacterium*, known homoacetogenic bacteria, can utilize H_2 and CO_2 to produce acetate [25,52]. Then, acetate can be consumed by either acetoclastic archaea or anodic electroactive bacteria [7,10,53]. The enrichment of *Acetobacterium* on

the stainless-steel mesh cathode electrode is an indicator to the occurrence of high HER in CF-SS, as compared to CF-CF. As mentioned earlier, H_2 gas has not been observed in the biogas samples in this study. This might be due to the rapid utilization of the generated H_2 via hydrogenotrophic methanogens or homoacetogenic *Acetobacterium*, as suggested in the literature [11,42]. In addition, the presence of the highest acetate concentration (439±2 mg COD/L) in CF-SS collaborated with a higher abundance of *Acetobacterium*. Moreover, *Acetobacterium* can help to maintain a lower hydrogen partial pressure to provide thermodynamically favorable conditions for propionate and butyrate fermentation to acetate. This notion is also supported in part by the lower propionate concentrations in CF-SS compared to the CF-CF.

3.6.2. Archaeal primer sequencing

For the archaeal phylum sequenced using specific archaeal primers, the abundance of Euryarchaeota were 32% and 51% at CF-CF and CF-SS, respectively (see Supporting Information). At the genus level, the abundance of *Methanobacterium* was almost similar in the anode biofilms of CF-CF and CF-SS (13% vs. 14%) (see Fig. 9b). However, *Methanobacterium* in cathode biofilms of CF-SS represented higher abundance than CF-CF (51% vs. 32%). Several studies revealed enrichment of known hydrogenotrophic methanogens, such as *Methanobacterium* and *Methanobrevibacter* in the cathode, which corroborated faster methanogenesis rates in MEC-AD systems over conventional digesters [8–11]. The superior HER kinetics on the stainless-steel cathode electrode (CF-SS) could enrich more hydrogenotrophic methanogens in CF-SS. Thus, the enhanced methane recovery from the CF-SS reactor can be explained by the high enrichment of *Methanobacterium*.

3.6.3. *mcr*A primer sequencing

Moreover, *mcr*A gene sequencing was performed to investigate the diversity and phylogeny of methanogens in both systems (Fig. 9c). The sequencing of the *mcr*A gene has been used previously in a few studies to understand the taxonomy of methanogens [33,50,51]. For the anodic biofilms, the abundance of *Methanobacterium* species were almost similar, including *formicicum* (CF-CF 67% vs. CF-SS 71%), and *subterraneum* (CF-CF 34% vs. CF-SS 29%). For the cathodic biofilms, CF-SS showed more diverse species of *Methanobacterium*; *formicicum* (54%), *subterraneum* (24.4%), and *palustre* (22%), as compared to CF-CF; *formicicum* (81%), and *subterraneum* (19%). Based on previous reports, electrotrophic activity of various species from the genus *Methanobacterium* is still uncertain [54–56]. Thus, the presence of diverse species of strict hydrogenotrophic *Methanobacterium* on CF-SS may have contributed to the faster utilization of hydrogen.

3.6.4. Principal component analysis

Fig. 11 shows the PCA analysis of biocathode bacterial and archaeal communities in two reactors using weighted Unifrac metrics to show the relation between genera and PCs. Based on 16S rRNA primer for bacterial sequencing of biocathode, the better performance of CF-SS was directly related to the enrichment of homoacetogenic *Acetobacterium* (Fig. 11a). However, the other genera might have an indirect relation to the superior performance of CF-SS. Based on specific archaeal primer for archaeal sequencing of biocathode, hydrogen-consuming *Methanobacterium* and *Acetobacterium* primarily contributed to the superior performance of stainless steel biocathode (Fig. 11b).

3.6.5. Expression patterns of EET genes

Fig. 12 shows the gene expression for *pil*A and c-type cytochromes (*omc*B, *omc*C, *omc*E, *omc*Z, and *omc*S). These genes showed trivial differences in expression levels in anode biofilms between both reactors, suggesting that higher current density from the CF-SS reactor was not attributed to

the overexpression of genes regulating anodic EET. The EET from EAB to the anode has been demonstrated to be facilitated via c-type cytochromes and conductive nanowire or pili [57], while fundamental aspects of EET mechanisms in methanogenic biocathode (i.e., direct electron transport from the electrode to methanogens) is still not well understood. Previous reports postulated that conductive pili and c-type cytochromes could play an important role in EET to electrotrophic methanogens from DIET-partners (i.e., electroactive bacteria) [55,58]. Based on the authors' knowledge, this study also first reports the expression of EET genes for methanogenic biocathode. Compared to anode biofilms, the EET-associated genes were less expressed in cathode biofilms in both reactors. Previous studies reported that some bacteria (e.g., *Enterobacteriaceae*, *Desulfovibrio*, etc.) found in cathode biofilms in this study could express different cytochromes and/or conductive pili [57,59]. Furthermore, a recent study suggested that *Methanobacterium* species could produce methane via DIET [60]. Nonetheless, the expression of these genes was quite comparable in both carbon fibers and stainless-steel cathode electrodes. Thus, the regulations of the EET genes were not affected by different electrode materials and were closely similar in expression levels. Hence, we can consider that differences in performances (i.e., current density, methane production) between two systems may be correlated to the HER and hydrogen utilization kinetics.

3.7 Implications

To the best of the authors' knowledge, the results of this study first present characteristics of EPS and expressions of EET genes in methanogenic biocathode grown on carbon fiber and stainless steel biocathode. As compared to the carbon fiber biocathode, a significantly higher EPS content as well as a higher abundance of *mcr*A gene copies, H_2-utilizing archaea, and homoacetogens were observed in the stainless steel biocathode. The effective catalysis of HER on stainless steel cathode

was appeared to be the primary reason behind the higher methane productivity and kinetics. Notably, the enrichment of homoacetogens appeared to be triggered by elevated HER on stainless steel cathode and served as a critical factor balancing HER, fermentation of metabolites (i.e., propionate), and methanogenesis process. It is known that proton reduction to hydrogen during HER will prompt local alkaline pH on the cathode. Hence, we can speculate that the highest EPS secretion in stainless steel biocathode could be linked with protecting cells from pH changes, as evidenced by the lowest ROS level than observed on carbon fiber biocathode. Thus, the results also provide new insights and suggest the importance of biocathode EPS as a potential area for further investigation of MEC-AD systems. However, gene expression patterns and redox activity of biocathode-derived EPS provided evidence that cathodic EET was also involved in methanogenesis in both biocathodes.

Regarding the engineering significance of the results, carbon-based electrodes have been mostly used as a biocathode material in MEC-AD systems due to their excellent biocompatibility and higher surface area over metal-based electrodes [3,24–26]. While carbon fibers provided a higher specific surface area, stainless steel mesh outperformed carbon fibers as a biocathode operated under similar operating conditions (e.g., anode electrode, inoculum, mixing, etc.). The results differ from our existing approach to designing MEC-AD systems by providing a high specific surface area of electrodes. Given that most of the single-chamber MEC-AD studies used carbon-based biocathode, the results of this study are significant for selecting efficient biocathode material to realize improved performance. However, it should be noted that the results presented here are from specific operating conditions with two selected electrode materials. Hence, further research is warranted with more carbon and metal electrodes with similar textures and surface areas.

Associated Content

Supporting Information: Estimation of specific surface area of carbon fiber and stainless-steel mesh electrode; EPS extraction protocol; EPS composition using CER and heating methods; Analytical methods for different EPS components; CLSM of reactive oxygen species (ROS); RT-PCR of gene expression levels; Primers used for studying gene expression levels; Microbial quantification using RT-PCR; The diversity and richness of the biofilms of both systems; Relative abundance of microbial community. Bacterial primer phylum level (a), and archaeal primer phylum level (b).

Acknowledgements

This work was supported by the Discovery Grant from Natural Sciences and Engineering Research Council of Canada (NSERC) and the Early Career Research Award from Future Energy Systems (FES). Basem Zakaria acknowledges Killam Trusts for Izaak Walton Killam Memorial Scholarship for his doctoral studies at the University of Alberta.

Contribution Statement

Basem S. Zakaria: Conceptualization, experiment, data analysis, writing - original draft, review/edit; **Bipro Ranjan Dhar:** Conceptualization, funding acquisition, project administration, supervision, writing/review/edit

Notes

The authors declare no competing financial interest.

References

(1) Park, J.; Lee, B.; Tian, D.; Jun, H. Bioelectrochemical Enhancement of Methane Production from Highly Concentrated Food Waste in a Combined Anaerobic Digester and Microbial Electrolysis Cell. *Bioresour. Technol.* **2018**, *247*, 226–233.

(2) Zakaria, B. S.; Dhar, B. R. An Intermittent Power Supply Scheme to Minimize Electrical Energy Input in a Microbial Electrolysis Cell Assisted Anaerobic Digester. *Bioresour. Technol.* **2021**, *319*, 124109.

(3) Choi, K. S.; Kondaveeti, S.; Min, B. Bioelectrochemical Methane (CH4) Production in Anaerobic Digestion at Different Supplemental Voltages. *Bioresour. Technol.* **2017**, *245*, 826–832.

(4) Huang, Q.; Liu, Y.; Dhar, B. R. A Critical Review of Microbial Electrolysis Cells Coupled with Anaerobic Digester for Enhanced Biomethane Recovery from High-Strength Feedstocks. *Crit. Rev. Environ. Sci. Technol.* **2020**.

(5) Zakaria, B. S.; Lin, L.; Chung, T.; Dhar, B. R. An Overview of Complementary Microbial Electrochemical Technologies for Advancing Anaerobic Digestion; Elsevier, 2020; Vol. 5, pp 129–167.

(6) Villano, M.; Aulenta, F.; Ciucci, C.; Ferri, T.; Giuliano, A.; Majone, M. Bioelectrochemical Reduction of CO2 to CH4 via Direct and Indirect Extracellular Electron Transfer by a Hydrogenophilic Methanogenic Culture. *Bioresour. Technol.* **2010**, *101* (9), 3085–3090.

(7) Zakaria, B. S.; Dhar, B. R. Progress towards Catalyzing Electro-Methanogenesis in Anaerobic Digestion Process: Fundamentals, Process Optimization, Design and Scale-up

Considerations. *Bioresource Technology*. Elsevier Ltd October 1, 2019, p 121738.

(8) Siegert, M.; Yates, M. D.; Spormann, A. M.; Logan, B. E. Methanobacterium Dominates Biocathodic Archaeal Communities in Methanogenic Microbial Electrolysis Cells. *ACS Sustain. Chem. Eng.* **2015**, *3* (7), 1668–1676.

(9) Siegert, M.; Li, X.-F.; Yates, M. D.; Logan, B. E. The Presence of Hydrogenotrophic Methanogens in the Inoculum Improves Methane Gas Production in Microbial Electrolysis Cells. *Front. Microbiol.* **2014**, *5* (DEC), 778.

(10) Cheng, S.; Xing, D.; Call, D. F.; Logan, B. E. Direct Biological Conversion of Electrical Current into Methane by Electromethanogenesis. *Environ. Sci. Technol.* **2009**, *43* (10), 3953–3958.

(11) Dykstra, C. M.; Pavlostathis, S. G. Methanogenic Biocathode Microbial Community Development and the Role of Bacteria. *Environ. Sci. Technol.* **2017**, *51* (9), 5306–5316.

(12) Zhang, L.; Zhu, X.; Li, J.; Liao, Q.; Ye, D. Biofilm Formation and Electricity Generation of a Microbial Fuel Cell Started up under Different External Resistances. *J. Power Sources* **2011**, *196* (15), 6029–6035.

(13) Zakaria, B. S.; Dhar, B. R. Changes in Syntrophic Microbial Communities, EPS Matrix, and Gene-Expression Patterns in Biofilm Anode in Response to Silver Nanoparticles Exposure. *Sci. Total Environ.* **2020**, *734*, 139395.

(14) Xiao, Y.; Zhang, E.; Zhang, J.; Dai, Y.; Yang, Z.; Christensen, H. E. M.; Ulstrup, J.; Zhao, F. Extracellular Polymeric Substances Are Transient Media for Microbial Extracellular Electron Transfer. *Sci. Adv.* **2017**, *3* (7), e1700623.

(15) Tian, T.; Qiao, S.; Yu, C.; Zhou, J. Effects of Nano-Sized MnO2 on Methanogenic

Propionate and Butyrate Degradation in Anaerobic Digestion. *J. Hazard. Mater.* **2019**, *364*, 11–18.

(16) Rollefson, J. B.; Stephen, C. S.; Tien, M.; Bond, D. R. Identification of an Extracellular Polysaccharide Network Essential for Cytochrome Anchoring and Biofilm Formation in Geobacter Sulfurreducens. *J. Bacteriol.* **2011**, *193* (5), 1023–1033.

(17) Tan, B.; Zhou, S. F.; Wang, Y.; Zhang, B. P.; Zhou, L. H.; Yuan, Y. Molecular Insight into Electron Transfer Properties of Extracellular Polymeric Substances of Electroactive Bacteria by Surface-Enhanced Raman Spectroscopy. *Sci. China Technol. Sci.* **2019**, *62* (10), 1679–1687.

(18) Ye, J.; Hu, A.; Ren, G.; Chen, M.; Tang, J.; Zhang, P.; Zhou, S.; He, Z. Enhancing Sludge Methanogenesis with Improved Redox Activity of Extracellular Polymeric Substances by Hematite in Red Mud. *Water Res.* **2018**, *134*, 54–62.

(19) Yu, H. Q. Molecular Insights into Extracellular Polymeric Substances in Activated Sludge. *Environ. Sci. Technol.* **2020**, *54* (13), 7742–7750.

(20) Villano, M.; Ralo, C.; Zeppilli, M.; Aulenta, F.; Majone, M. Influence of the Set Anode Potential on the Performance and Internal Energy Losses of a Methane-Producing Microbial Electrolysis Cell. *Bioelectrochemistry* **2016**, *107*, 1–6.

(21) Ma, X.; Li, Z.; Zhou, A.; Yue, X. Energy Recovery from Tubular Microbial Electrolysis Cell with Stainless Steel Mesh as Cathode. *R. Soc. Open Sci.* **2017**, *4* (12), 170967.

(22) Guo, Z.; Thangavel, S.; Wang, L.; He, Z.; Cai, W.; Wang, A.; Liu, W. Efficient Methane Production from Beer Wastewater in a Membraneless Microbial Electrolysis Cell with a Stacked Cathode: The Effect of the Cathode/Anode Ratio on Bioenergy Recovery. *Energy*

and Fuels **2017**, *31* (1), 615–620.

(23) Noori, M. T.; Vu, M. T.; Ali, R. B.; Min, B. Recent Advances in Cathode Materials and Configurations for Upgrading Methane in Bioelectrochemical Systems Integrated with Anaerobic Digestion. *Chemical Engineering Journal*. Elsevier B.V. July 15, 2020, p 123689.

(24) Liu, W.; Cai, W.; Guo, Z.; Wang, L.; Yang, C.; Varrone, C.; Wang, A. Microbial Electrolysis Contribution to Anaerobic Digestion of Waste Activated Sludge, Leading to Accelerated Methane Production. *Renew. Energy* **2016**, *91*, 334–339.

(25) Liu, D.; Zheng, T.; Buisman, C.; Ter Heijne, A. Heat-Treated Stainless Steel Felt as a New Cathode Material in a Methane-Producing Bioelectrochemical System. *ACS Sustain. Chem. Eng.* **2017**, *5* (12), 11346–11353.

(26) De Vrieze, J.; Gildemyn, S.; Arends, J. B. A.; Vanwonterghem, I.; Verbeken, K.; Boon, N.; Verstraete, W.; Tyson, G. W.; Hennebel, T.; Rabaey, K. Biomass Retention on Electrodes Rather than Electrical Current Enhances Stability in Anaerobic Digestion. *Water Res.* **2014**, *54*, 211–221.

(27) Kim, K. R.; Kang, J.; Chae, K. J. Improvement in Methanogenesis by Incorporating Transition Metal Nanoparticles and Granular Activated Carbon Composites in Microbial Electrolysis Cells. *Int. J. Hydrogen Energy* **2017**, *42* (45), 27623–27629.

(28) Park, J.; Lee, B.; Shin, W.; Jo, S.; Jun, H. Application of a Rotating Impeller Anode in a Bioelectrochemical Anaerobic Digestion Reactor for Methane Production from High-Strength Food Waste. *Bioresour. Technol.* **2018**, *259*, 423–432.

(29) Call, D. F.; Merrill, M. D.; Logan, B. E. High Surface Area Stainless Steel Brushes as

Cathodes in Microbial Electrolysis Cells. *Environ. Sci. Technol.* **2009**, *43* (6), 2179–2183.

(30) Wang, J.; Li, M.; Liu, F.; Chen, S. Stainless Steel Mesh Supported Carbon Nanofibers for Electrode in Bioelectrochemical System. *J. Nanomater.* **2016**, *2016*.

(31) Klindworth, A.; Pruesse, E.; Schweer, T.; Peplies, J.; Quast, C.; Horn, M.; Glöckner, F. O. Evaluation of General 16S Ribosomal RNA Gene PCR Primers for Classical and Next-Generation Sequencing-Based Diversity Studies. *Nucleic Acids Res.* **2013**, *41* (1), e1–e1.

(32) Logares, R.; Lindström, E. S.; Langenheder, S.; Logue, J. B.; Paterson, H.; Laybourn-Parry, J.; Rengefors, K.; Tranvik, L.; Bertilsson, S. Biogeography of Bacterial Communities Exposed to Progressive Long-Term Environmental Change. *ISME J.* **2013**, *7* (5), 937–948.

(33) Morris, R.; Schauer-Gimenez, A.; Bhattad, U.; Kearney, C.; Struble, C. A.; Zitomer, D.; Maki, J. S. Methyl Coenzyme M Reductase (McrA) Gene Abundance Correlates with Activity Measurements of Methanogenic H2/CO2-Enriched Anaerobic Biomass. *Microb. Biotechnol.* **2014**, *7* (1), 77.

(34) Caporaso, J. G.; Kuczynski, J.; Stombaugh, J.; Bittinger, K.; Bushman, F. D.; Costello, E. K.; Fierer, N.; Peña, A. G.; Goodrich, J. K.; Gordon, J. I.; Huttley, G. A.; Kelley, S. T.; Knights, D.; Koenig, J. E.; Ley, R. E.; Lozupone, C. A.; McDonald, D.; Muegge, B. D.; Pirrung, M.; Reeder, J.; Sevinsky, J. R.; Turnbaugh, P. J.; Walters, W. A.; Widmann, J.; Yatsunenko, T.; Zaneveld, J.; Knight, R. QIIME Allows Analysis of High-Throughput Community Sequencing Data. *Nat. Methods* **2010**, *7* (5), 335–336.

(35) Zakaria, B. S.; Lin, L.; Dhar, B. R. Shift of Biofilm and Suspended Bacterial Communities with Changes in Anode Potential in a Microbial Electrolysis Cell Treating Primary

Sludge. *Sci. Total Environ.* **2019**, *689*, 691–699.

(36) Li, S.; Cheng, C.; Thomas, A. Carbon-Based Microbial-Fuel-Cell Electrodes: From Conductive Supports to Active Catalysts. *Advanced Materials*. **2017**, 29, 1602547.

(37) He, G.; Gu, Y.; He, S.; Schröder, U.; Chen, S.; Hou, H. Effect of Fiber Diameter on the Behavior of Biofilm and Anodic Performance of Fiber Electrodes in Microbial Fuel Cells. *Bioresour. Technol.* **2011**, *102* (22), 10763–10766.

(38) Champigneux, P.; Delia, M. L.; Bergel, A. Impact of Electrode Micro- and Nano-Scale Topography on the Formation and Performance of Microbial Electrodes. *Biosensors and Bioelectronics*. Elsevier Ltd October 30, 2018, 231–246.

(39) Babapoor, A.; Azizi, M.; Karimi, G. Thermal Management of a Li-Ion Battery Using Carbon Fiber-PCM Composites. *Appl. Therm. Eng.* **2015**, *82*, 281–290.

(40) Gaby, J. C.; Zamanzadeh, M.; Horn, S. J. The Effect of Temperature and Retention Time on Methane Production and Microbial Community Composition in Staged Anaerobic Digesters Fed with Food Waste. *Biotechnol. Biofuels* **2017**, *10* (1), 302.

(41) Krylova, N. I.; Conrad, R. Thermodynamics of Propionate Degradation in Methanogenic Paddy Soil. *FEMS Microbiol. Ecol.* **1998**, *26* (4), 281–288.

(42) Asztalos, J. R.; Kim, Y. Enhanced Digestion of Waste Activated Sludge Using Microbial Electrolysis Cells at Ambient Temperature. *Water Res.* **2015**, *87*, 503–512.

(43) Stöckl, M.; Teubner, N. C.; Holtmann, D.; Mangold, K. M.; Sand, W. Extracellular Polymeric Substances from Geobacter Sulfurreducens Biofilms in Microbial Fuel Cells. *ACS Appl. Mater. Interfaces* **2019**, *11* (9), 8961–8968.

(44) Park, J.-H.; Kang, H.-J.; Park, K.-H.; Park, H.-D. Direct Interspecies Electron Transfer via

Conductive Materials: A Perspective for Anaerobic Digestion Applications. *Bioresour. Technol.* **2018**, *254*, 300–311.

(45) Yang, G.; Huang, L.; Yu, Z.; Liu, X.; Chen, S.; Zeng, J.; Zhou, S.; Zhuang, L. Anode Potentials Regulate Geobacter Biofilms: New Insights from the Composition and Spatial Structure of Extracellular Polymeric Substances. *Water Res.* **2019**, *159*, 294–301.

(46) Cerrillo, M.; Viñas, M.; Bonmatí, A. Overcoming Organic and Nitrogen Overload in Thermophilic Anaerobic Digestion of Pig Slurry by Coupling a Microbial Electrolysis Cell. *Bioresour. Technol.* **2016**, *216*, 362–372.

(47) Cai, W.; Liu, W.; Zhang, Z.; Feng, K.; Ren, G.; Pu, C.; Sun, H.; Li, J.; Deng, Y.; Wang, A. McrA Sequencing Reveals the Role of Basophilic Methanogens in a Cathodic Methanogenic Community. *Water Res.* **2018**, *136*, 192–199.

(48) Wormald, R.; Humphreys, P. Hydrogenotrophic Methanogenesis Dominates at High PH. *Access Microbiol.* **2019**, *1* (1A), 169.

(49) Zheng, L.; Zhang, Z.; Tian, L.; Zhang, L.; Cheng, S.; Li, Z.; Cang, D. Mechanistic Investigation of Toxicological Change in ZnO and TiO2 Multi-Nanomaterial Systems during Anaerobic Digestion and the Microorganism Response. *Biochem. Eng. J.* **2019**, *147*, 62–71.

(50) Wilkins, D.; Lu, X. Y.; Shen, Z.; Chen, J.; Lee, P. K. H. Pyrosequencing of McrA and Archaeal 16s RRNA Genes Reveals Diversity and Substrate Preferences of Methanogen Communities in Anaerobic Digesters. *Appl. Environ. Microbiol.* **2015**, *81* (2), 604–613.

(51) Alonso, R. M.; Escapa, A.; Sotres, A.; Morán, A. Integrating Microbial Electrochemical Technologies with Anaerobic Digestion to Accelerate Propionate Degradation. *Fuel* **2020**,

267, 117158.

(52) Dhar, B. R.; Park, J. H.; Park, H. D.; Lee, H. S. Hydrogen-Based Syntrophy in an Electrically Conductive Biofilm Anode. *Chem. Eng. J.* **2019**, *359*, 208–216.

(53) Fu, Q.; Kuramochi, Y.; Fukushima, N.; Maeda, H.; Sato, K.; Kobayashi, H. Bioelectrochemical Analyses of the Development of a Thermophilic Biocathode Catalyzing Electromethanogenesis. *Environ. Sci. Technol.* **2015**, *49* (2), 1225–1232.

(54) Batlle-Vilanova, P.; Puig, S.; Gonzalez-Olmos, R.; Vilajeliu-Pons, A.; Balaguer, M. D.; Colprim, J. Deciphering the Electron Transfer Mechanisms for Biogas Upgrading to Biomethane within a Mixed Culture Biocathode. *RSC Adv.* **2015**, *5* (64), 52243–52251.

(55) Rotaru, A.-E.; Shrestha, P. M.; Liu, F.; Shrestha, M.; Shrestha, D.; Embree, M.; Zengler, K.; Wardman, C.; Nevin, K. P.; Lovley, D. R. A New Model for Electron Flow during Anaerobic Digestion: Direct Interspecies Electron Transfer to Methanosaeta for the Reduction of Carbon Dioxide to Methane. *Energy Environ. Sci.* **2014**, *7* (1), 408–415.

(56) Xu, H.; Wang, K.; Holmes, D. E. Bioelectrochemical Removal of Carbon Dioxide (CO2): An Innovative Method for Biogas Upgrading. *Bioresour. Technol.* **2014**, *173*, 392–398.

(57) Hernández-Eligio, A.; Pat-Espadas, A. M.; Vega-Alvarado, L.; Huerta-Amparán, M.; Cervantes, F. J.; Juárez, K. Global Transcriptional Analysis of Geobacter Sulfurreducens under Palladium Reducing Conditions Reveals New Key Cytochromes Involved. *Appl. Microbiol. Biotechnol.* **2020**, *104* (9), 4059–4069.

(58) Park, J.-H.; Park, J. H.; Je Seong, H.; Sul, W. J.; Jin, K. H.; Park, H. D. Metagenomic Insight into Methanogenic Reactors Promoting Direct Interspecies Electron Transfer via Granular Activated Carbon. *Bioresour. Technol.* **2018**, *259*, 414–422.

(59) Gardy, J. L.; Spencer, C.; Wang, K.; Ester, M.; Tusnády, G. E.; Simon, I.; Hua, S.; deFays, K.; Lambert, C.; Nakai, K.; Brinkman, F. S. L. PSORT-B: Improving Protein Subcellular Localization Prediction for Gram-Negative Bacteria. *Nucleic Acids Res.* **2003**, *31* (13), 3613–3617.

(60) Zheng, S.; Liu, F.; Wang, B.; Zhang, Y.; Lovley, D. R. Methanobacterium Capable of Direct Interspecies Electron Transfer. *Environ. Sci. Technol.* **2020**, *54*, 15347–15354.

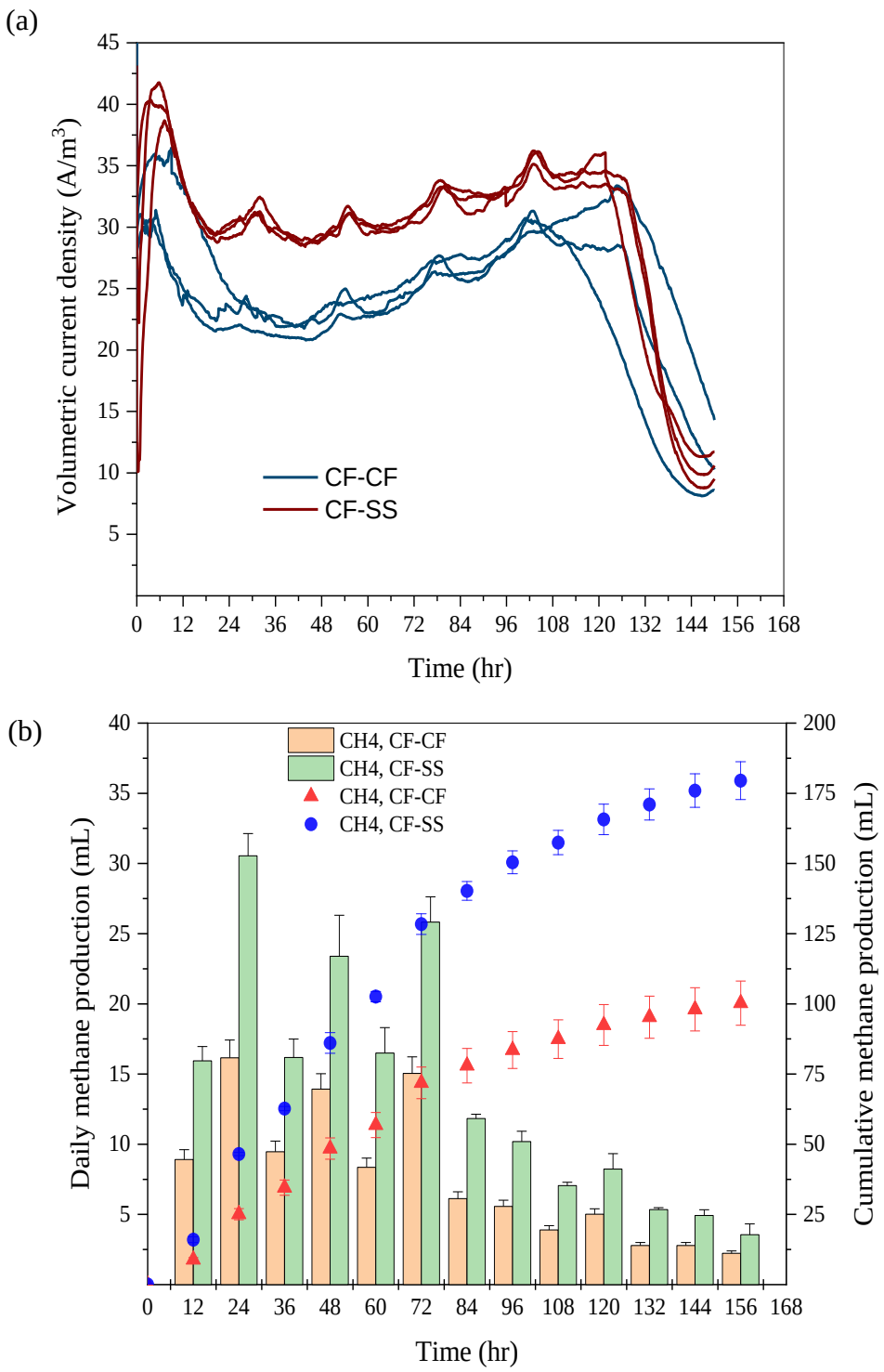

Fig. 1. Volumetric current density (a), and methane production (b) from CF-CF and CF-SS reactors. Note. The results from 3 representative batch cycles during steady-state were shown. The error bars indicate the standard deviation of three replicates (n = 3).

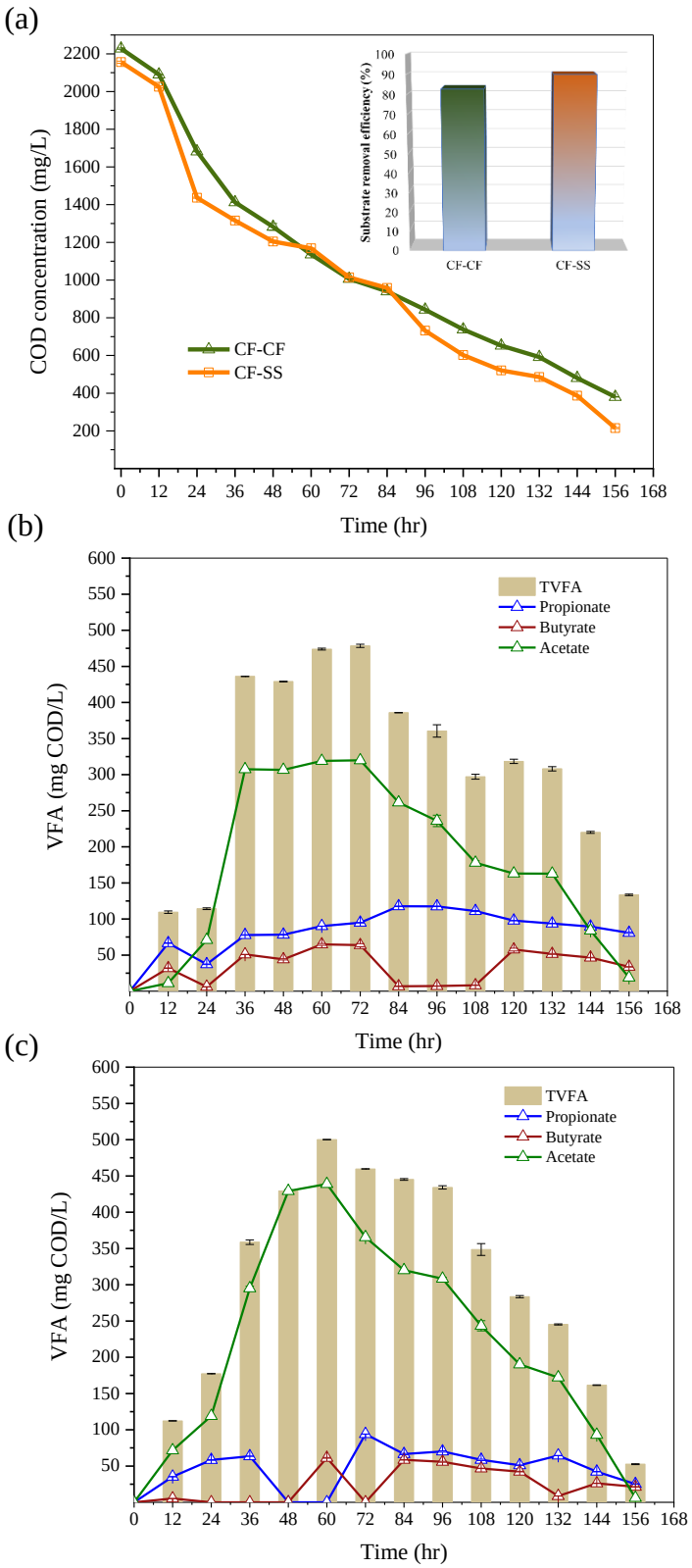

Fig. 2. COD concentration (a), and VFA profiles (b, c) in CF-CF and CF-SS reactors. The error bars show the standard deviation of three replicates (n = 3).

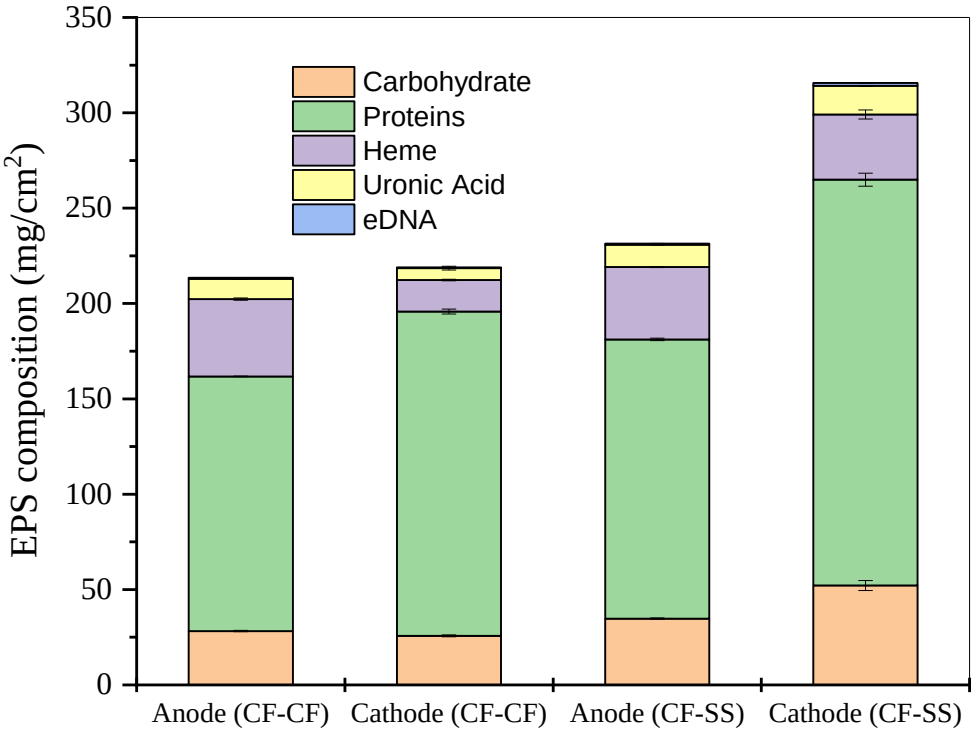

Fig. 3. EPS composition of CF-CF and CF-SS reactors. Note. The error bars indicate the standard deviation of three replicates (n = 3).

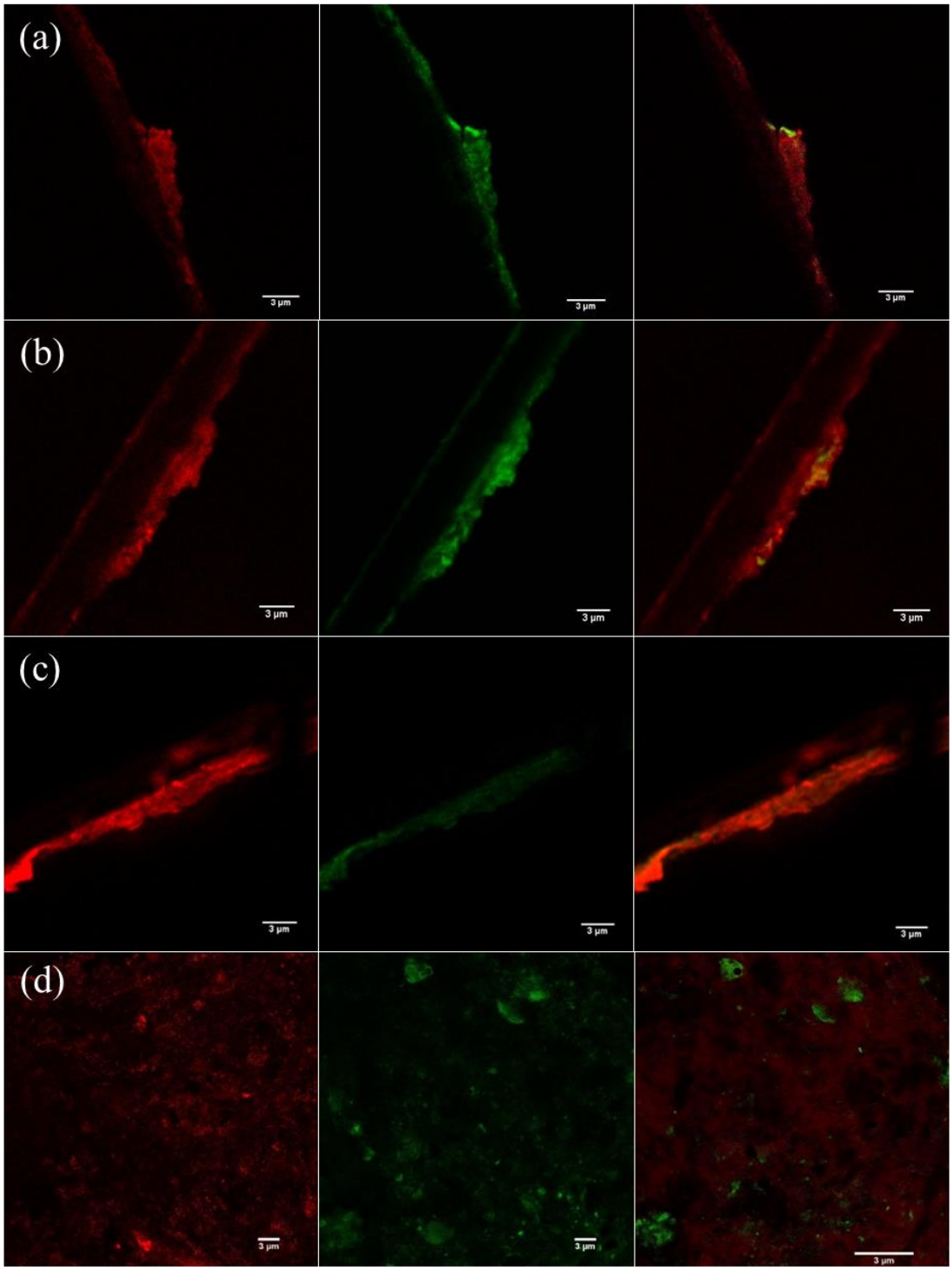

Fig. 4. Representative confocal microscopic images of EPS with 3 µm scale; anode (CF-CF) (a), cathode (CF-CF) (b), anode (CF-SS) (c), and cathode (CF-SS) (d). The green color represents eDNA and the red color indicates EPS.

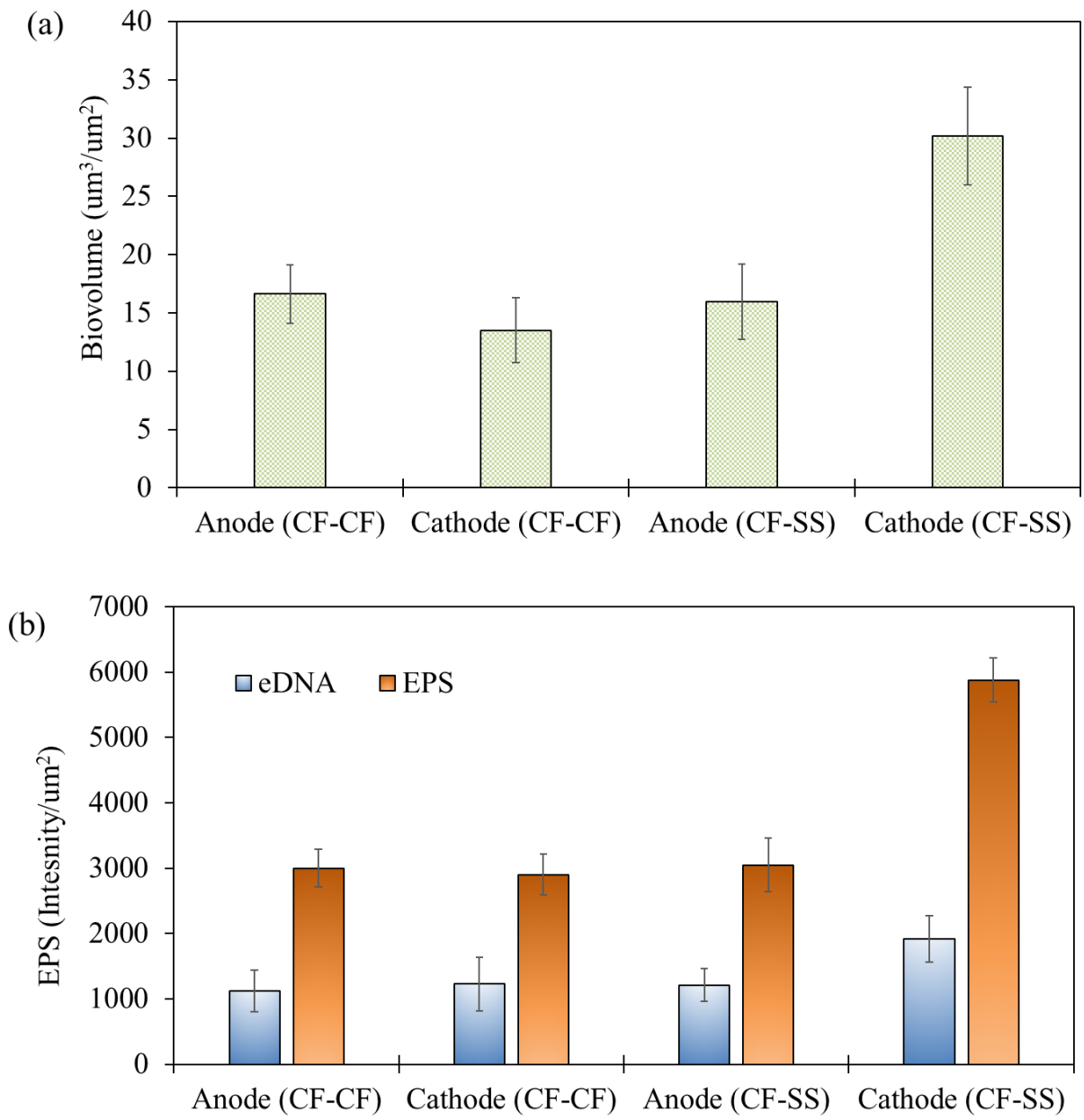

Fig. 5. EPS quantitative analysis using CLSM; biovolume (a), and fluorescence intensity (b). The error bars indicate the standard deviation of three replicates (n = 3).

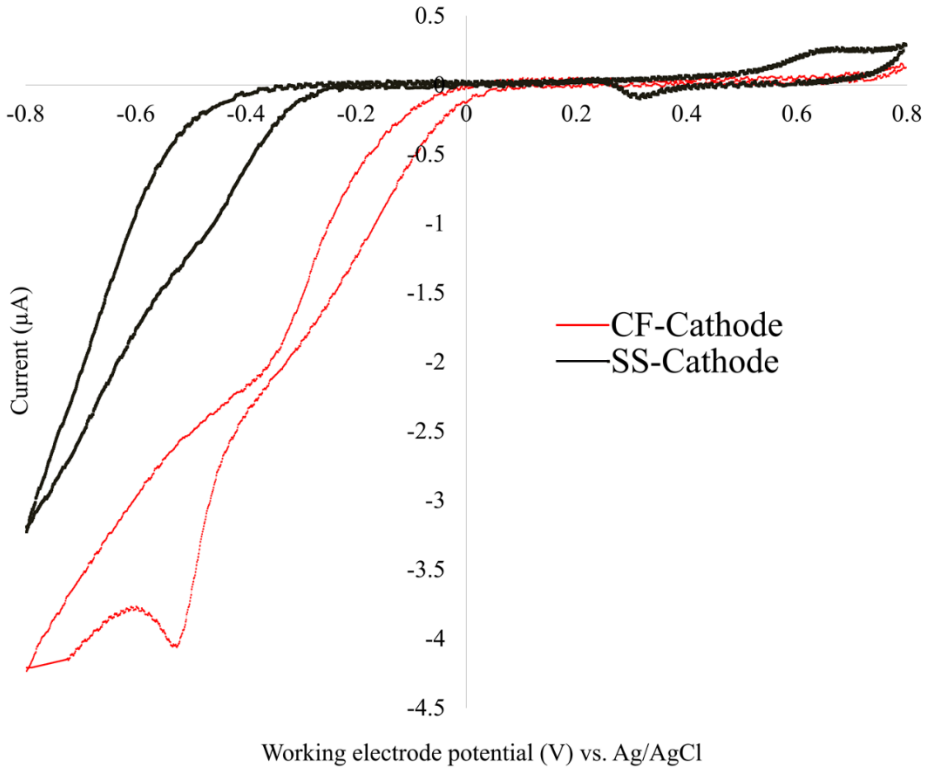

Fig. 6. Cyclic voltammetry of EPS extracted from biocathode in CF-CF and CF-SS reactors.

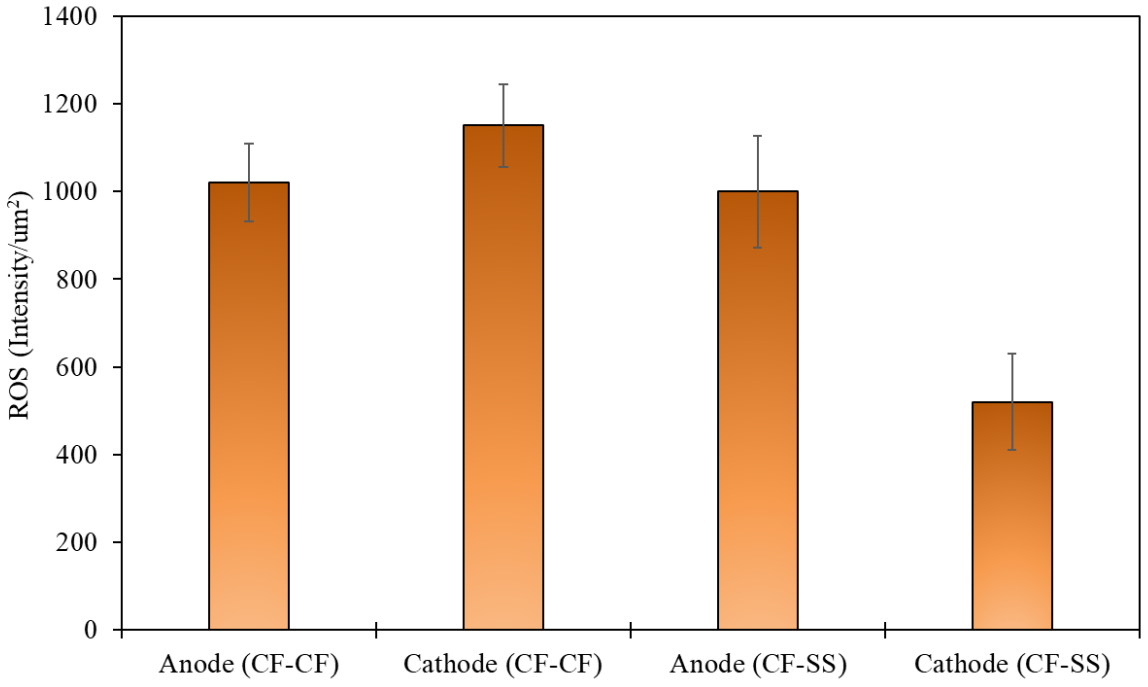

Fig. 7. Reactive oxygen species (ROS) intensities in CF-CF and CF-SS biofilms. The error bars indicate the standard deviation of three replicates (n = 3).

(a)

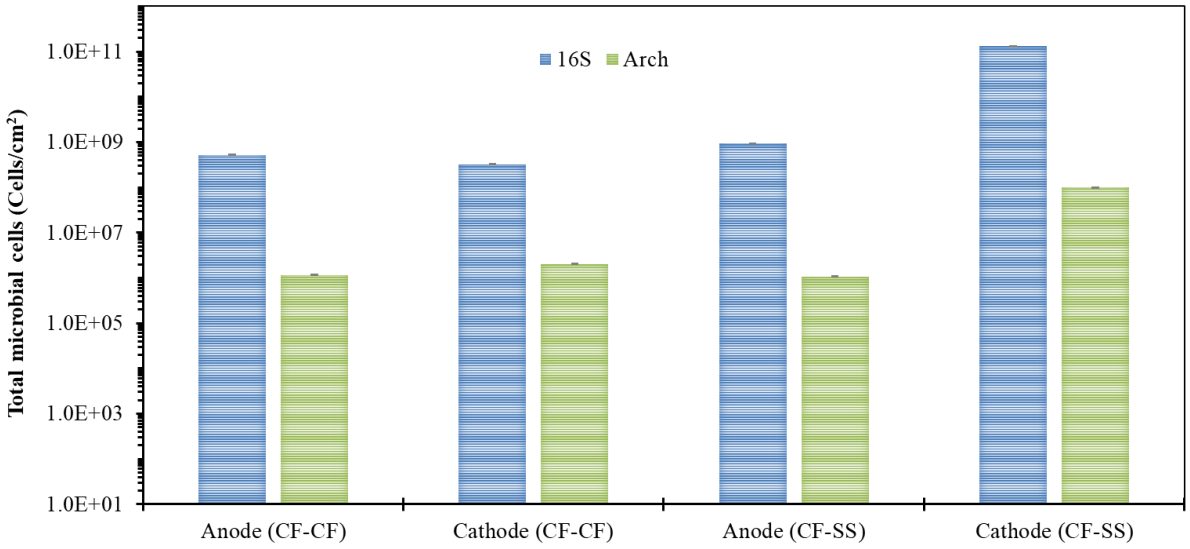

(b)

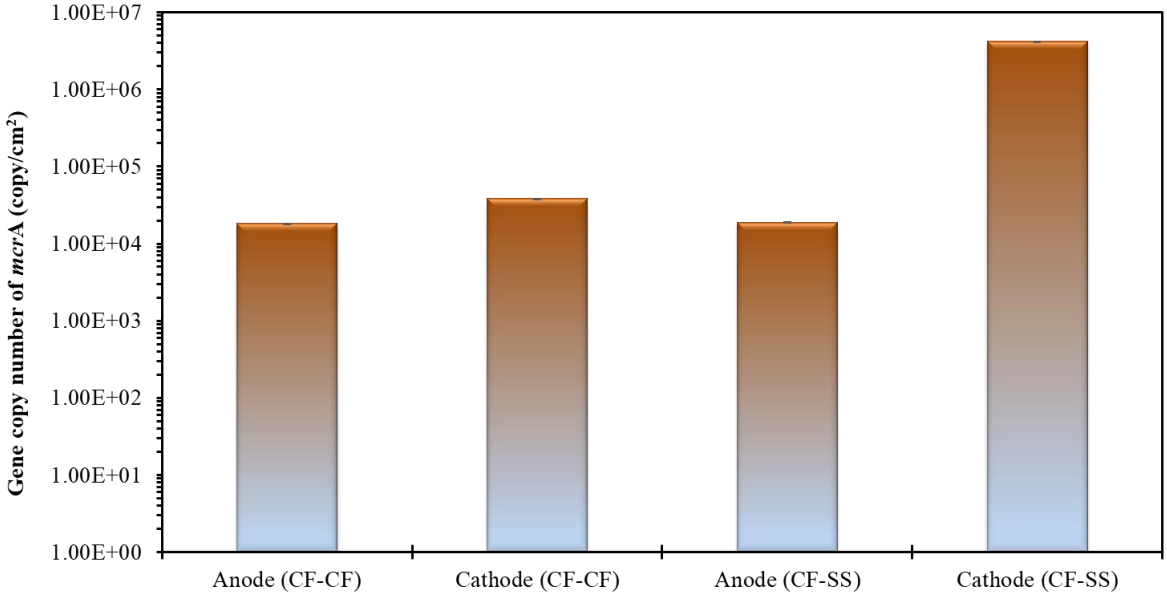

Fig. 8. Total cell number using 16s and archaeal primers (a), and *mcr*A gene copies (b). The error bars indicate the standard deviation of three replicates (n = 3).

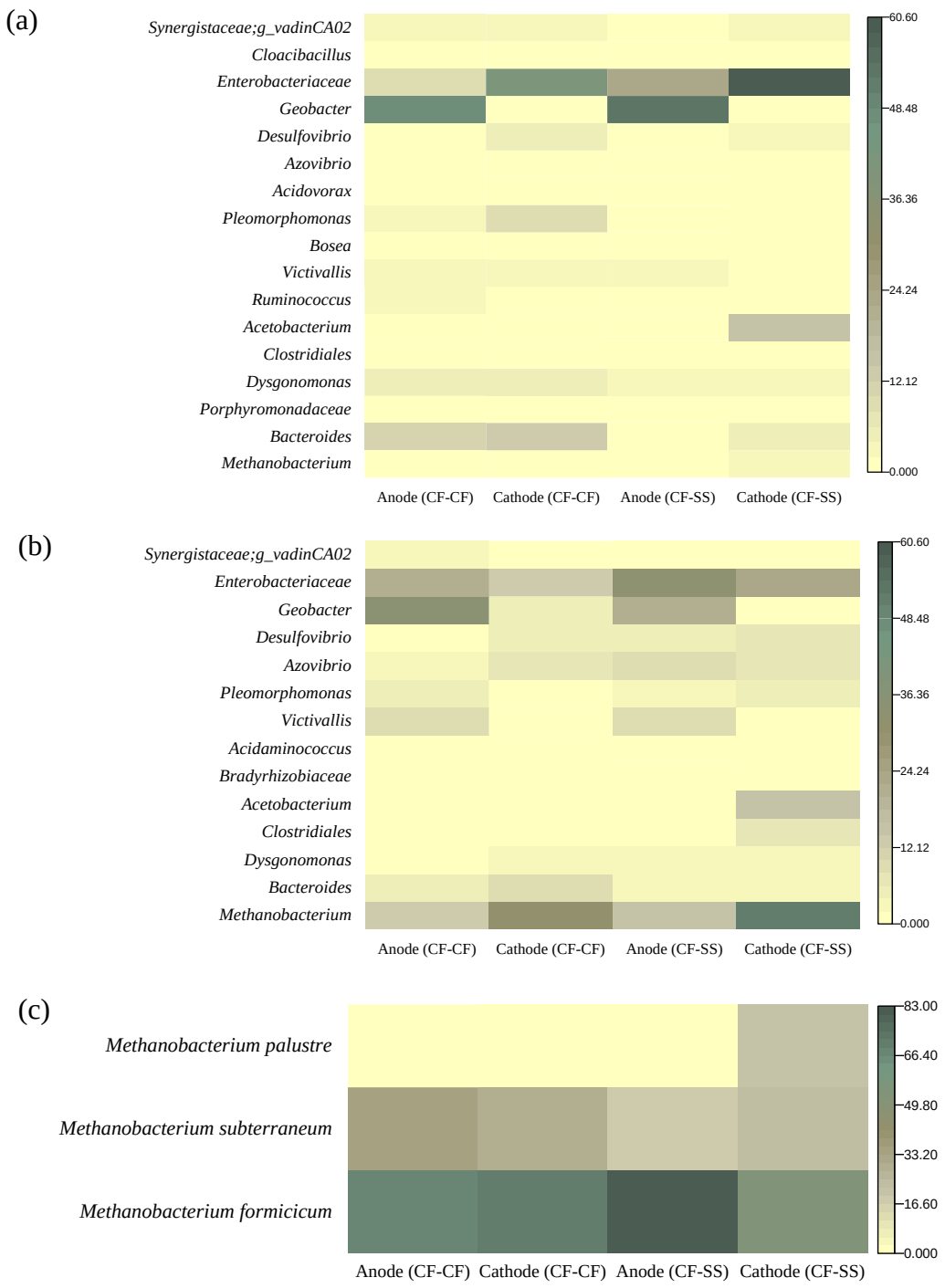

Fig. 9. Relative abundance of microbial communities analyzed with bacterial primer (a), archaeal primer (b), and *mcr*A primer (c) at the genus level.

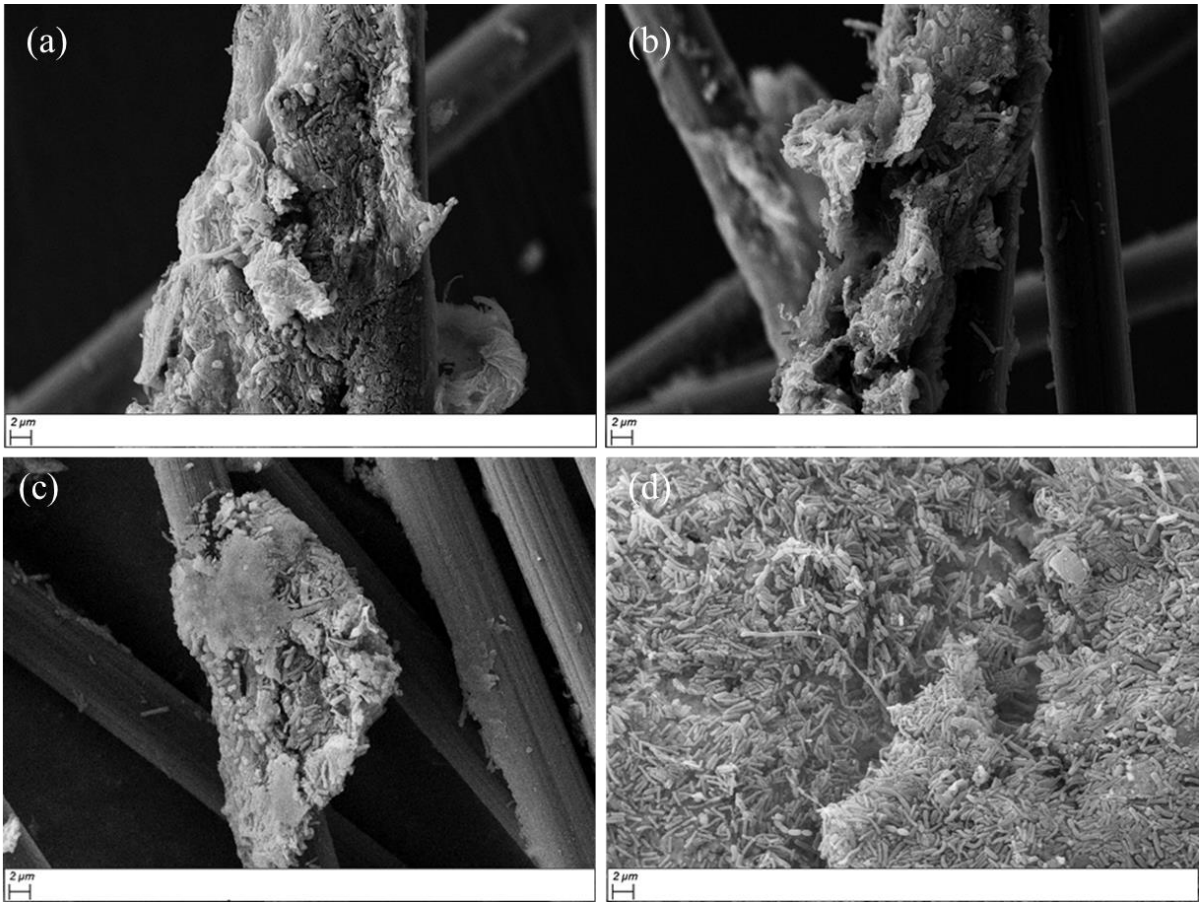

Fig. 10. Representative SEM images of biofilms developed on anode (CF-CF) (a), cathode (CF-CF) (b), anode (CF-SS) (c), and cathode (CF-SS) (d).

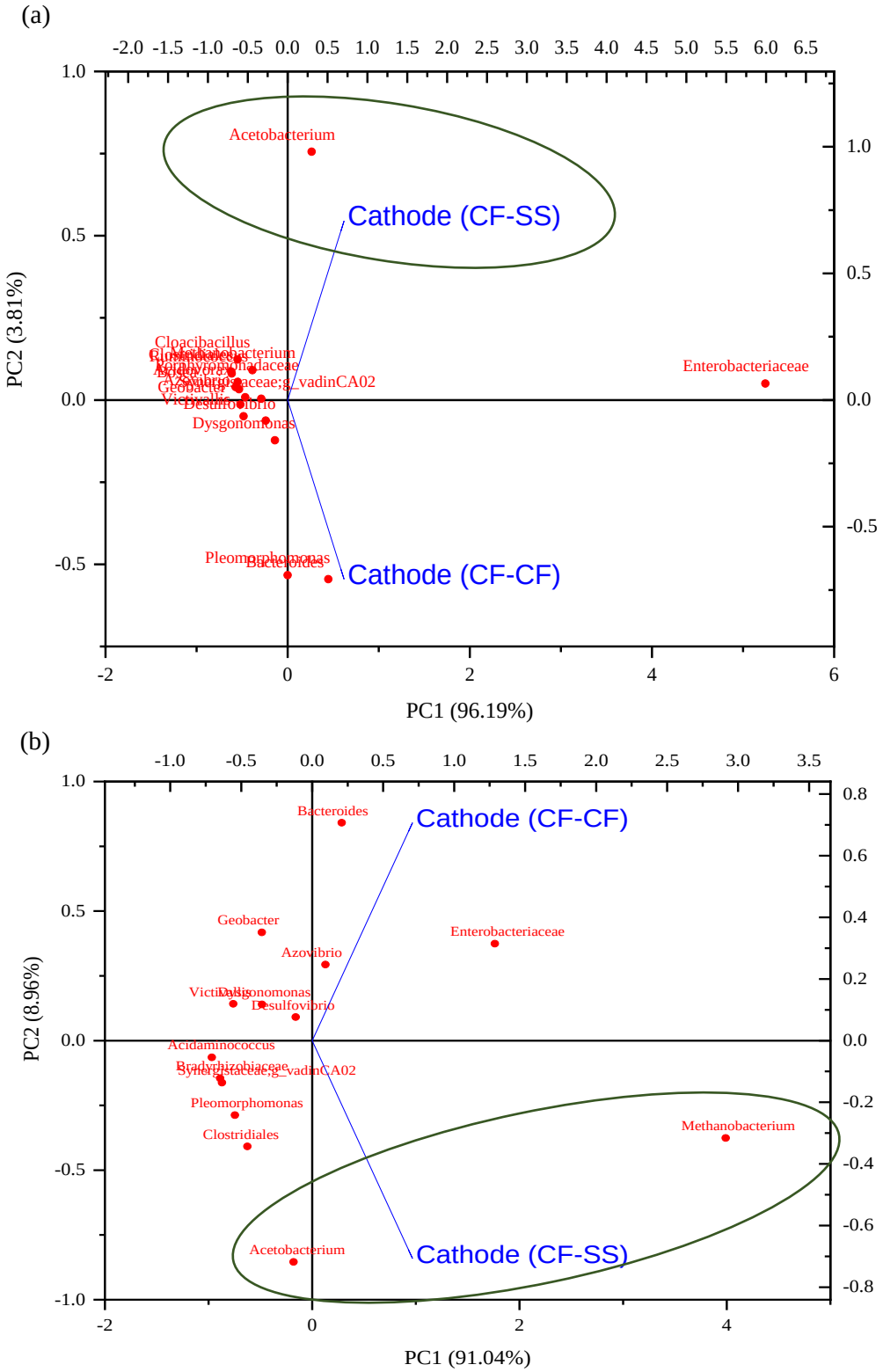

Fig. 11. Principal Component Analysis of the bacterial (a) and archaeal (b) communities in biocathode of CF-CF and CF-SS reactors.

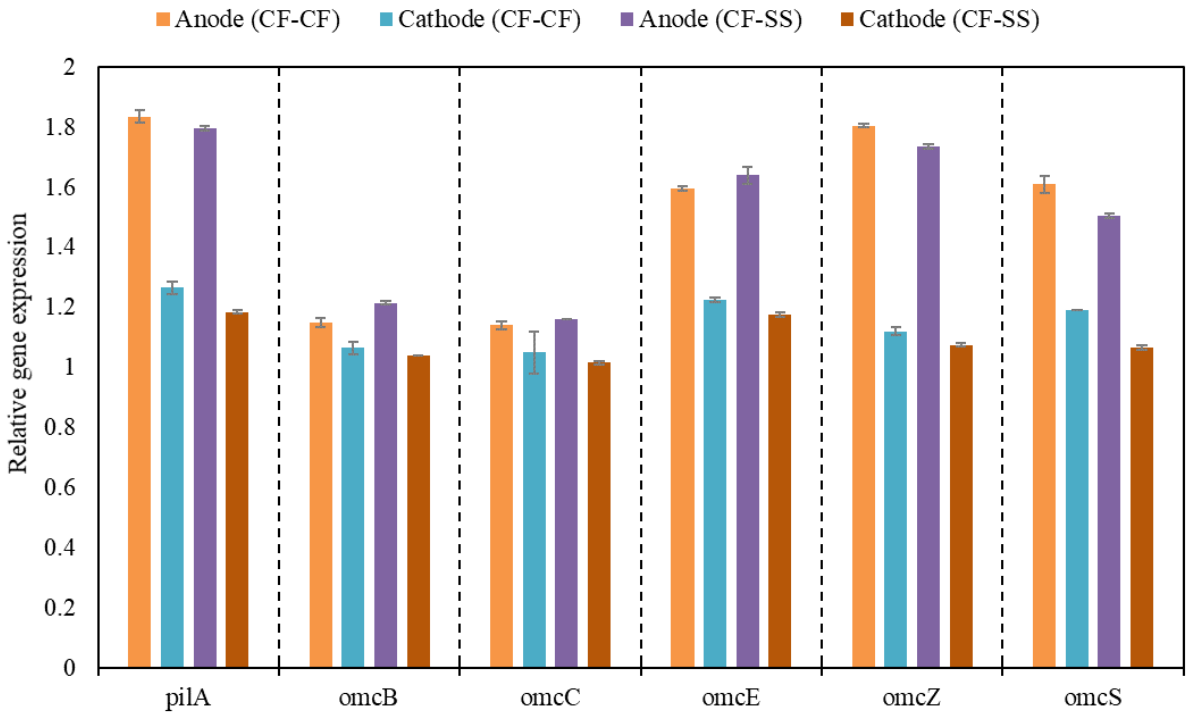

Fig. 12. Expression of genes known to regulate extracellular electron transfer in biofilms. The error bars indicate the standard deviation of three replicates (n = 3).

Supplementary Information

Significance of extracellular polymeric substances, reactive oxygen species, and expression of extracellular electron transfer genes on methanogenic activity in biocathode

Basem S. Zakaria, Bipro Ranjan Dhar*

Civil and Environmental Engineering, University of Alberta, 9211-116 Street NW, Edmonton, AB, Canada T6G 1H9

*Corresponding author: Bipro Ranjan Dhar (bipro@ualberta.ca)

Number of pages: 13

Number of figures: 3

Number of tables: 3

Text S1. Estimation of specific surface area of carbon fiber and stainless-steel mesh electrode

1. Stainless-steel mesh electrode

The surface area was calculated according to Zhang et al. [1] with minor modification.

$$S = 2\pi b d n(n+1) + \frac{3}{2}\pi d^2 (n+1)^2$$

Where, (b) is the pore size, and (d) is the wire diameter, (n) is 70 mesh

b= 0.02 cm, d = 0.016 cm

The specific surface area based on reactor volume = 0.0016 m^2/0.00038 m^3 = 4.23 m^2/m^3

2. Carbon fiber electrode

The surface area of carbon fiber was calculated using two approaches previously reported in the literature [2,3]:

1. Considering every single filament in the carbon fiber bundle (filament bundle consists of 24000 single filaments, each with diameter 7 µm, and the length = 130 cm)

S.A. = 2πrh x n = 2 x 3.14 x 0.0007 cm x 130 cm x 24000 = 13715.5 cm^2

The specific surface area based on reactor volume = 1.372 m^2 / 0.00038 m^3 = 3609 m^2/m^3

2. Considering all filaments in a bundle act together as a single fiber (width = 0.5 cm, length = 130 cm, height = 0.1 cm).

S.A.= 2 (wh +Lw + Lh) = 156.4 cm^2

The specific surface area based on reactor volume = 0.0156 m^2 / 0.00038 m^3 = 41 m^2/m^3

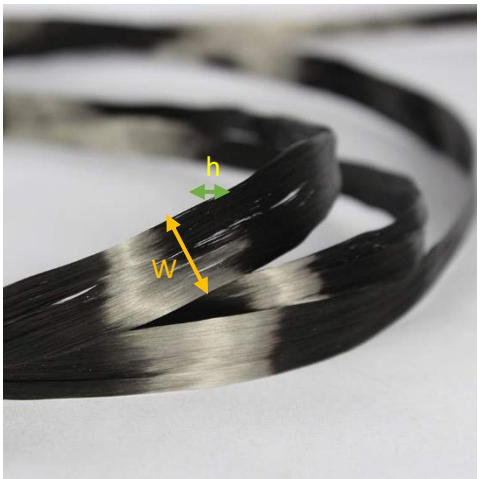

Fig. S1. Photograph of carbon fiber bundle.

Text S2. EPS extraction protocol: CER method for EPS extraction was performed according to Frølund et al. [4] with some minor modification, 52 cm^2 of carbon fiber and 0.054 cm^2 of stainless-steel were resuspended in 0.1 M PBS buffer, pH 7.4. Then, 2 g CER (Dowex® Marathon® C sodium form, Sigma-Aldrich, USA), washed with 0.1 M PBS for 15 min (10 mL g^{-1} Dowex), was added to each sample. The samples were agitated at a high capacity for 20 min on the shaker (Vortex Mixer, Fisher Scientific, USA). The heating method was conducted according to Xu et al. [5], the electrodes were washed twice with 0.9% NaCl (w/v), then resuspended in 0.9% NaCl (w/v). The samples were heated at 60°C in a water bath for 30 minutes. For both methods, the EPS were harvested by centrifugation three times at 20,000 × g for 20 minutes at 4°C. The supernatant was collected and filtered using a 0.2 µm filter and the EPS stored at -20°C for further analysis. Also, the pellets were collected to examine the cell lysis using Glucose-6-Phosphate Dehydrogenase kit (Sigma-Aldrich, USA).

Table S2. EPS composition using CER and heating methods.

	Carbohydrate	**Proteins**	**Heme**	**Uronic Acid**	**eDNA**
CER Method					
Anode (CF-CF)	28.225	133.545	40.58	10.6	0.55
Cathode (CF-CF)	25.775	170.025	16.52	6.2	0.39
Anode (CF-SS)	34.775	146.405	37.94	11.665	0.685
Cathode (CF-SS)	52.14	212.79	34.22	15	1.525
Heating Method					
Anode (CF-CF)	35.575	109.29	50.45	13.065	0.69
Cathode (CF-CF)	27.78	163.29	18.62	8.27	0.365
Anode (CF-SS)	24.1	172.855	41.13	11.32	0.46
Cathode (CF-SS)	52.61	223.885	37.57	15.2	1.715

Text S3. Analytical methods for different EPS components: The total carbohydrate content was measured using a phenol-sulfuric acid method using glucose standards according to DuBois et al. [6] with some minor modification. 2 mL of EPS was mixed with 5 mL of concentrated sulfuric acid followed by the addition of 0.05 mL of 80% wt. phenol. Then, the samples were incubated at room temperature for 10 minutes, then shake followed by incubation for 20 minutes at 30ºC. The samples were measured at 490 nm using UV-spectrophotometer (Model DR 3900, HACH, Germany). The protein contents of the EPS were measured using Pierce™ Modified Lowry Protein Assay Kit (Thermo Fisher, USA) according to the manufacturer's instructions. Uronic acid was measured according to Blumenkrantz and Asboe-Hansen [7] and Ghods et al. [8] with glucuronic acid (Sigma-Aldrich, USA) as a standard. Heme contents were measured using the Heme Assay Kit (Heme Assay Kit, Sigma-Aldrich, USA) according to the manufacturer's instructions. The extracellular DNA (eDNA) was quantified using the diphenylamine colorimetric method with calf thymus DNA as the standard [9]. 100 µL EPS was pipetted in a cuvette and 2.5 mL of the reagent (0.2 ppm DAPI (4, 6-diaminodino-2-phenylindole) in 100 mM NaC1, l0 mM EDTA, 10 mM PBS, pH 7.2) was added. All the above measurements were conducted in triplicate.

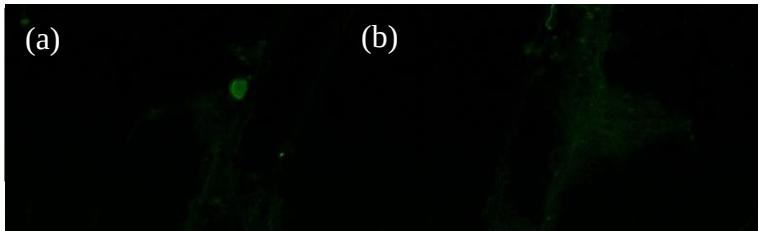

Fig. S2. CLSM of reactive oxygen species (ROS). Anode (CF-CF) (a), cathode (CF-CF) (b), anode (CF-SS) (c), and cathode (CF-SS) (d).

Text S4. RT-PCR of gene expression levels. The concept is to design primers to detect most of the *omc*B, *omc*C, *omc*E, *omc*Z, *omc*S, and *pil*A gene sequences as possible. The primer design was performed similarly to Lin et al. [10], and *rec*A housekeeping gene was used as a reference [11]. The genome sequences of the anode biofilm were collected from the National Center for Biotechnology Information (NCBI) (https://www.ncbi.nlm.nih.gov). These followed by multiple-aligned using the ClustalX alignment tool (http://www.clustal.org/clustal2/) to select most of the homologous gene regions [12]. Then, gene-specific primers for RT-PCR were designed with Primer3 software (http://bioinfo.ut.ee/primer3) by selecting an almost similar range of melting temperatures. The Basic Local Alignment Search Tool (BLAST) (https://blast.ncbi.nlm.nih.gov/Blast.cgi) was used to check the specificity of the primers. Also, the primers were experimentally examined using agarose gel electrophoresis. The primers were prepared by Integrated DNA Technologies (IDT, USA) and are listed in Table S1.

Table S1. Primers used for studying gene expression levels

	Forward (5'-3')	Reverse (5'-3')
*rec*A	CACCGGCATAATCTCCAAGT	ATCTTGCGGATATCGAGACG
*pil*A	TTATGATCGTGGTTGCCATT	CCGCAGTTAAACCTTCTGCT
	GAGCGATGTTCTTTCCGTTT	AATCCTGATAGGCGGGAATC
omcB	CCGAAAATTACGCAGGTGTT	GGAGTTCACGAAACCAAGGA
	GAGGGACGATGTCAACCTGT	TTCGCAAGGTAGCTGTTGTG
omcC	CTGGTACTCTGGGTGGCATT	GCTGTGGTTAGCAGCATTGA
	ACGAGTTCCAGACCAACACC	GGCAGTATCGTCCCAGTTGT
omcE	ATGTCCTACGGCGATGCTAT	GTAACCTGCAGGAAGGTGGA
	CTCGTCCAGCAGCATGAATA	GGGGTGATCATTGCTCAGAT
omcZ	GGACGTATTGTGGCAGAGGT	GGCCACTACATTCCGACCTA
	GGCCACTACATTCCGACCTA	GGACGTATTGTGGCAGAGGT
omcS	GCTGACTACACCGTGCTCAA	TGAACTCGTATGCCAGGTTG
	GGCAAGTACCGTCGTTTTGT	GTAGCTTCCGTCCGGTTGTA

Text S5. Microbial quantification using RT-PCR. qPCR was performed to quantify bacterial cell numbers before and after AgNPs injection. 16S universal primers, 357Wf: CCTACGGGNGGCWGCAG and 785R: GACTACHVGGGTATCTAATCC, were used to quantify the DNA samples. qPCR mixtures were prepared in 25 uL reactions using QuantiFast SYBR® Green PCR Kit (Qiagen, CA) as the following: 2 µL of the DNA template, 12.5 µL 2x master mix, 2.5 µL forward and reverse specific primer, and 5.5 µL nuclease-free water. CFX 96 real-time PCR system with a C1000 Thermal Cycler (Bio-Rad, USA) was used with the following cycling conditions according to the QuantiFast SYBR® Green PCR Kit's protocol; PCR initial heat activation cycle at 95 ˚C for 5 min, 35 cycles at 95 ˚C for 10 sec and 60 ˚C for 30 sec, and finally, one cycle at 40 ˚C for 30 seconds. Triplicate reactions were run for all samples.

Table S3. The diversity and richness of the biofilms of both systems.

Reactor/electrode		Chao 1	Phylogenetic distance	OTUs	Pielou's evenness	Shannon	Coverage
CF-CF	**Anode**	137	11.68	132	0.45	3.14	1.0
	Cathode	76	7.19	76	0.63	3.95	1.0
CF-SS	**Anode**	146	13.57	146	0.72	5.18	1.0
	Cathode	155	12.32	150	0.71	5.10	1.0

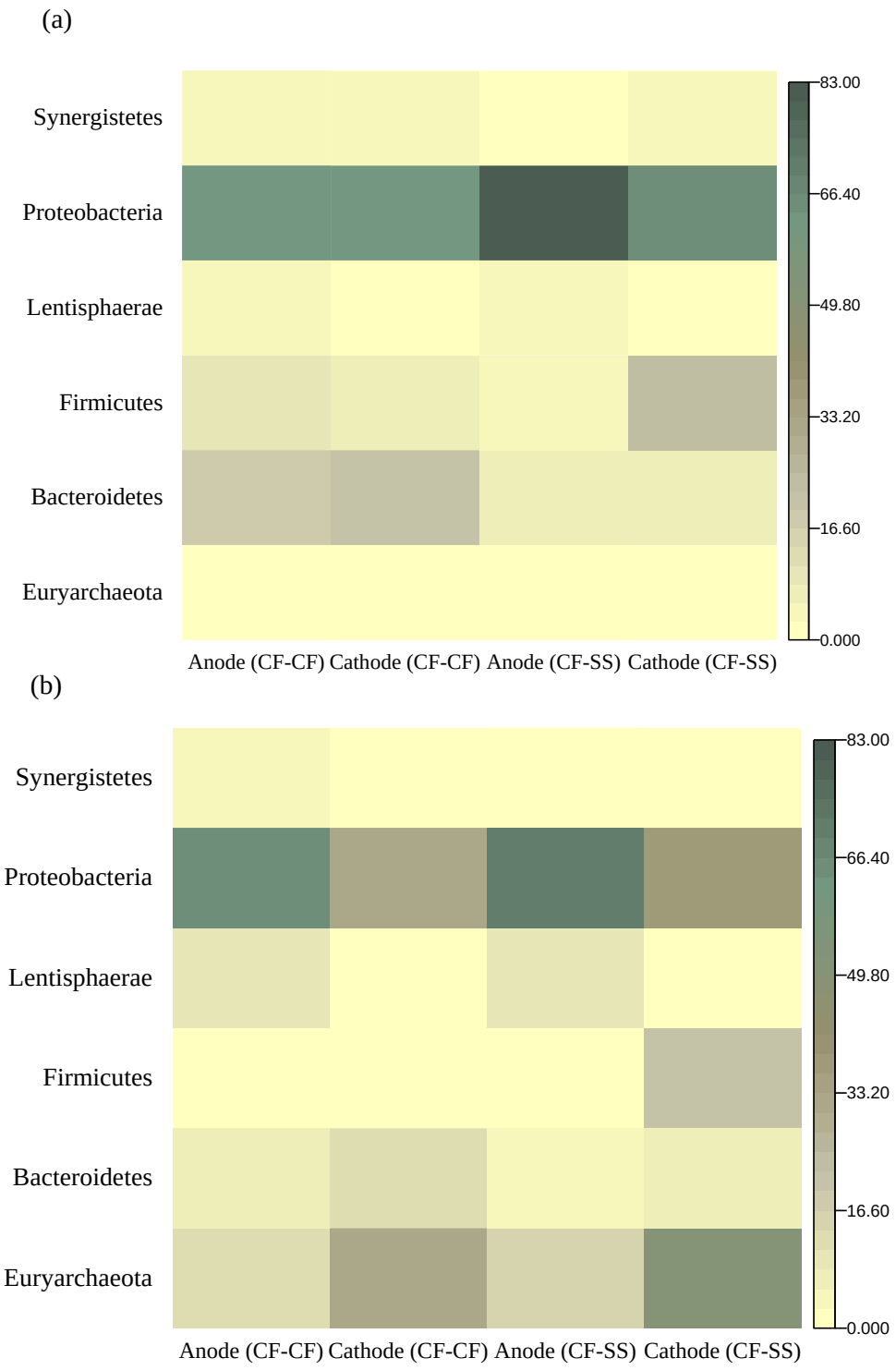

Fig. S3. Relative abundance of microbial community. Bacterial primer phylum level (a), and archaeal primer phylum level (b).

References

(1) Zhang, Y.; Merrill, M. D.; Logan, B. E. The Use and Optimization of Stainless Steel Mesh Cathodes in Microbial Electrolysis Cells. *Int. J. Hydrogen Energy* **2010**, *35* (21), 12020–12028.

(2) Brunschweiger, S.; Ojong, E. T.; Weisser, J.; Schwaferts, C.; Elsner, M.; Ivleva, N. P.; Haseneder, R.; Hofmann, T.; Glas, K. The Effect of Clogging on the Long-Term Stability of Different Carbon Fiber Brushes in Microbial Fuel Cells for Brewery Wastewater Treatment. *Bioresour. Technol. Reports* **2020**, *11*, 100420.

(3) Lanas, V.; Logan, B. E. Evaluation of Multi-Brush Anode Systems in Microbial Fuel Cells. *Bioresour. Technol.* **2013**, *148*, 379–385.

(4) Frølund, B.; Palmgren, R.; Keiding, K.; Nielsen, P. H. Extraction of Extracellular Polymers from Activated Sludge Using a Cation Exchange Resin. *Water Res.* **1996**, *30* (8), 1749–1758.

(5) Xu, J.; Sheng, G. P.; Ma, Y.; Wang, L. F.; Yu, H. Q. Roles of Extracellular Polymeric Substances (EPS) in the Migration and Removal of Sulfamethazine in Activated Sludge System. *Water Res.* **2013**, *47* (14), 5298–5306.

(6) DuBois, M.; Gilles, K. A.; Hamilton, J. K.; Rebers, P. A.; Smith, F. Colorimetric Method for Determination of Sugars and Related Substances. *Anal. Chem.* **1956**, *28* (3), 350–356.

(7) Blumenkrantz, N.; Asboe-Hansen, G. New Method for Quantitative Determination of Uronic Acids. *Anal. Biochem.* **1973**, *54* (2), 484–489.

(8) Ghods, S.; Sims, I. M.; Moradali, M. F.; Rehma, B. H. A. Bactericidal Compounds Controlling Growth of the Plant Pathogen Pseudomonas Syringae Pv. Actinidiae, Which Forms Biofilms Composed of a Novel Exopolysaccharide. *Appl. Environ. Microbiol.* **2015**, *81* (12), 4026–4036.

(9) Brunk, C. F.; Jones, K. C.; James, T. W. Assay for Nanogram Quantities of DNA in Cellular Homogenates. *Anal. Biochem.* **1979**, *92* (2), 497–500.

(10) Lin, L.; Chowdhury, B.; Zakaria, B. S.; Dhar, B. R. Temperature-Dependent (20–55 °C) Electrocatalytic Characteristics during Ethanol/Propionate Degradation by Methanogenic Communities Grown on Conductive Carbon Fibers. *Chem. Eng. J.* **2019**, 123566.

(11) Rivas, M.; Seeger, M.; Holmes, D. S.; Jedlicki, E. A Lux-like Quorum Sensing System in the Extreme Acidophile Acidithiobacillus Ferrooxidans. *Biol. Res.* **2005**, *38* (2–3), 283–297.

(12) Thompson, J. The CLUSTAL_X Windows Interface: Flexible Strategies for Multiple Sequence Alignment Aided by Quality Analysis Tools. *Nucleic Acids Res.* **1997**, *25* (24), 4876–4882.